



Review

Carbon Nanomaterials-Based Electrically Conductive Scaffolds to Repair the Ischaemic Heart Tissue

Arsalan Ul Haq^{1,2,*}, Felicia Carotenuto^{1,2}, Federica Trovalusci³, Fabio De Matteis^{2,4} and Paolo Di Nardo^{1,2}

¹ Department of Clinical Sciences and Translational Medicine, Faculty of Medicine and Surgery, University of Rome "Tor Vergata", Via Montpellier 1, 00133 Rome, Italy

² Interdepartmental Research Centre for Regenerative Medicine (CIMER), Department of Clinical Sciences and Translational Medicine, Faculty of Medicine and Surgery, University of Rome "Tor Vergata", Via Montpellier 1, 00133 Rome, Italy

³ Department of Business Engineering, Faculty of Engineering, University of Rome "Tor Vergata", Via del Politecnico 1, 00133 Rome, Italy

⁴ Department of Industrial Engineering, Faculty of Engineering, University of Rome "Tor Vergata", Via del Politecnico 1, 00133 Rome, Italy

* Correspondence: arsalan.ulhaq@students.uniroma2.eu

Abstract: Ischaemic heart diseases are the leading causes of morbidity around the world and pose serious socio-economic burdens. Ischaemic events, such as myocardial infarction, lead to severe tissue damage and result in the formation of scar tissue. This scar tissue, being electrically inert, does not conduct electrical currents and thus generates lethal arrhythmias. The ventricle dilates with time due to asynchronous beating due to the scar, and it eventually leads to total heart failure. The current pharmacological approaches only cure heart failure symptoms without inducing tissue regeneration. Therefore, heart transplant remains the gold standard to date, but the limited organ donors and the possibility of immune rejection make this approach elusive. Cardiac tissue engineering has the potential to address this issue by engineering artificial heart tissues using 3D scaffolds cultured with cardiac stem cells. Compared with the traditional non-conductive scaffold, electroconductive scaffolds can transfer feeble electric currents among the cultured cells by acting as a "wire". This improves intercellular communication and synchronisation that otherwise is not possible using non-conductive scaffolds. This article reviews the recent advances in carbon nanomaterials-based electroconductive scaffolds, their in vitro/in vivo efficacy, and their potential to repair ischaemic heart tissue.

Keywords: carbon nanomaterials; ischaemic tissue repair; myocardial infarction; electrically conductive scaffold; cardiac tissue engineering



Citation: Ul Haq, A.; Carotenuto, F.; Trovalusci, F.; De Matteis, F.; Di Nardo, P. Carbon Nanomaterials-Based Electrically Conductive Scaffolds to Repair the Ischaemic Heart Tissue. *C* **2022**, *8*, 72. <https://doi.org/10.3390/c8040072>

Academic Editor: Giuseppe Cirillo

Received: 31 October 2022

Accepted: 1 December 2022

Published: 4 December 2022

Publisher's Note: MDPI stays neutral with regard to jurisdictional claims in published maps and institutional affiliations.



Copyright: © 2022 by the authors. Licensee MDPI, Basel, Switzerland. This article is an open access article distributed under the terms and conditions of the Creative Commons Attribution (CC BY) license (<https://creativecommons.org/licenses/by/4.0/>).

1. Introduction

Ischaemic heart diseases (IHDs) are the leading cause of morbidity, with a relatively high death rate in the Western world (Figure 1). Its estimated global prevalence rate (1655/100 k people) is expected to exceed 1845/100 k people by 2030 [1]. Besides imposing severe economic burdens, IHDs also hamper the everyday life of the affected individuals. Myocardial infarction (MI) is one of the IHDs, and it is a consequence of coronary artery blockage delivering blood to the heart tissue. This blockage, due to blood clots/plaque, results in tissue ischaemia and the death of contractile cardiomyocytes (CMs) [2]. Once injured, the heart tissue cannot heal itself due to its poor innate regeneration capability, unlike some other tissues [3,4]. The injured area gets replaced with collagen-rich scar tissue, and this scar tissue, being electrically inert due to collagen, induces lethal arrhythmias that lead to total heart failure in the long run [5,6]. The current pharmacological approaches tend to reverse the dilation of the failing ventricle by activating anti-inflammatory pathways but do not induce the much-needed regeneration of the injured tissue [7–10]. Therefore, heart

transplant remains the gold standard so far, but the lack of organ donors and the possibility of immune rejection make this approach elusive.

Ischemic heart disease in Both Sexes, 2019

All Ages, Deaths Rate/100K

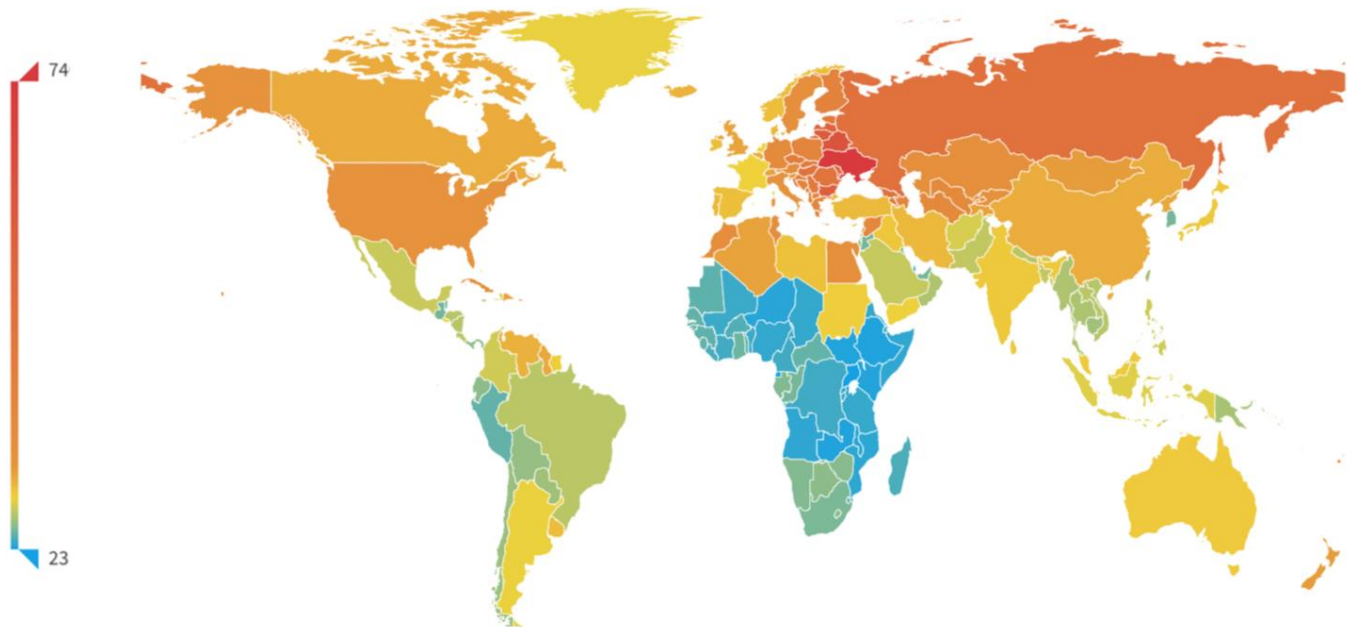


Figure 1. Global death rate due to ischaemic heart diseases. Source: Institute for Health Metrics Evaluation. Used with permission. All rights reserved.

Tissue engineering is a multidisciplinary field in which stem cells are seeded in a scaffold to engineer artificial tissues. A scaffold can be considered a 3D structure emulating the micro/nano bio-architectural features (mainly pore size) of an extracellular matrix (ECM) of a tissue [11]. These engineered tissues, cellular or acellular grafts, can be implanted *in vivo* to induce the regeneration of the injured area that cannot heal itself otherwise. The scaffolds that are normally implanted (with or without cells) at the infarct site tend to induce tissue regeneration [12], but they do not resolve the issues, such as arrhythmias, due to their non-conductive nature. To overcome this, inert biomaterials (natural or synthetic) can be blended with electrically conductive polymers (polyaniline, polypyrrole, or polythiophene) or carbon nanomaterials (CNTs, graphene, or nanofibers) to obtain an electrically conductive scaffold. This scaffold harnesses biocompatibility and mechanical properties from the non-conductive component (biomaterial) while the conductive component imparts electrical conductivity. This, in turn, can provide the cultured cardiac stem cells with proper bioelectrical cues to drive their differentiation and maturation towards cardiomyocyte-like cells with a contractile phenotype. The implantation of electrically conductive constructs at the infarct site has also significantly resolved the arrhythmic issues with improved blood pumping ability of the injured heart, as shown in rat MI models [13,14].

This article reviews the recent developments in the conductive scaffold-based cardiac tissue engineering approach using carbon nanomaterials (CNMs) as the conductive component of the scaffold. The myocardial infarction, its consequences, and the *in vitro/in vivo* efficacy of CNMs-based conductive scaffolds as potential candidates to resolve MI-related issues are schematically shown in Figure 2.

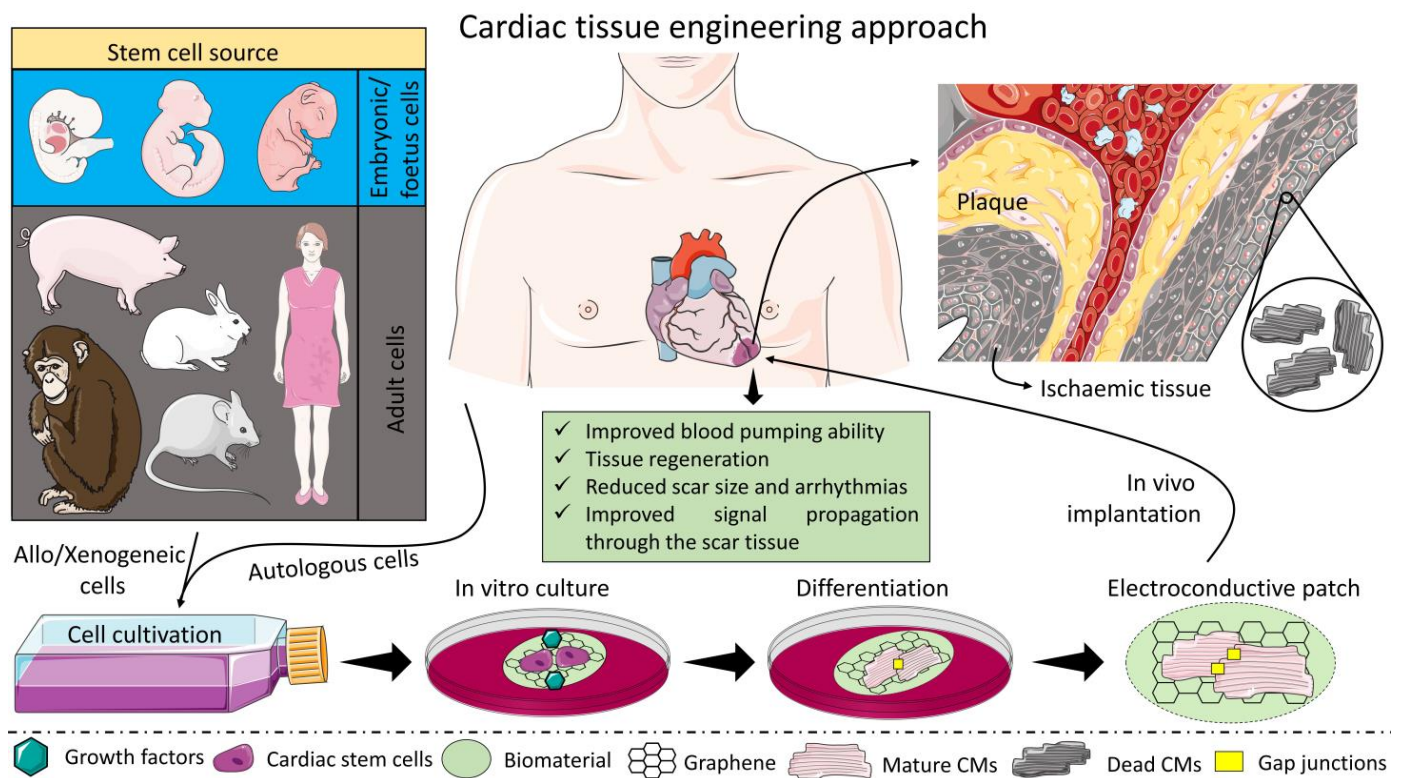


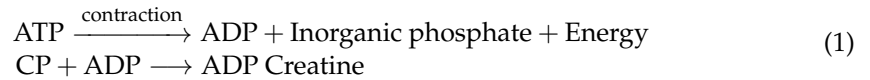
Figure 2. Electroconductive scaffold-based cardiac tissue engineering approach to repair ischaemic tissue. Figure was made using the images from the Servier Medical Art.

2. The Contractile Machinery of the Heart

The heart is a muscular organ that pumps blood through the entire body. Cardiomyocytes (CMs), also known as “the contractile machinery of the heart”, are the building blocks of the contractile myocardium, as shown in Figure 3. The perpetual contraction-relaxation of the heart is maintained by action potentials (APs) that travel from one CM to another through gap junctions, thus maintaining efficient electrical signal transmission. Adenosine triphosphate (ATP) fuels the contractile function of the cardiomyocyte, and it is produced through two main processes (i) anaerobic glycolysis and (ii) aerobic respiration. Glycolysis, which takes place in the cytosol, produces a small amount of ATP with pyruvate. Lactate is also formed from pyruvate because glycolysis and lactate dehydrogenase (LDH) maintain the concentration balance between pyruvate and lactate [15]. A large amount of ATP is produced through aerobic respiration involving the complex Krebs cycle and oxidative phosphorylation processes in the mitochondria. This ATP is then used as fuel to conduct certain intracellular processes.

The contraction begins when the action potential from adjacent cardiomyocytes activates the voltage-gated calcium channels on the plasma membrane of CM. This results in the influx of the extracellular Ca^{2+} through these channels activating ryanodine receptor channels on the sarcoplasmic reticulum (SR). The release of a large number of stored Ca^{2+} from SR results in a sudden increase in the calcium levels in the cell thus creating a calcium spark. This spark generates a calcium signal which allows Ca^{2+} to attach to the troponin present on the tropomyosin filaments. The attachment of calcium ions to troponin exposes the binding sites for the myosin head to attach to actin filaments. An ATP molecule is attached to each myosin head which then slides the actin filament. The sliding of all actin filaments at once generates rhythmic contractions. After contraction, the ATP is converted into adenosine diphosphate (ADP) and inorganic phosphate. The ATP supply of the muscle

is consumed quickly, and it is renewed when creatine phosphate (CP) donates a high energy phosphate to ADP as shown in Equation (1).



Creatine is then filtered through the kidneys and excreted out of the body via the urinary system. When cardiomyocyte relaxes after contraction calcium ions leave the troponin and are pumped back to the sarcoplasmic reticulum for storage. Ion exchangers maintain a continuous exchange between sodium and calcium ions across the plasma membrane while the sodium-potassium pump keeps the optimum ionic gradient in the cell.

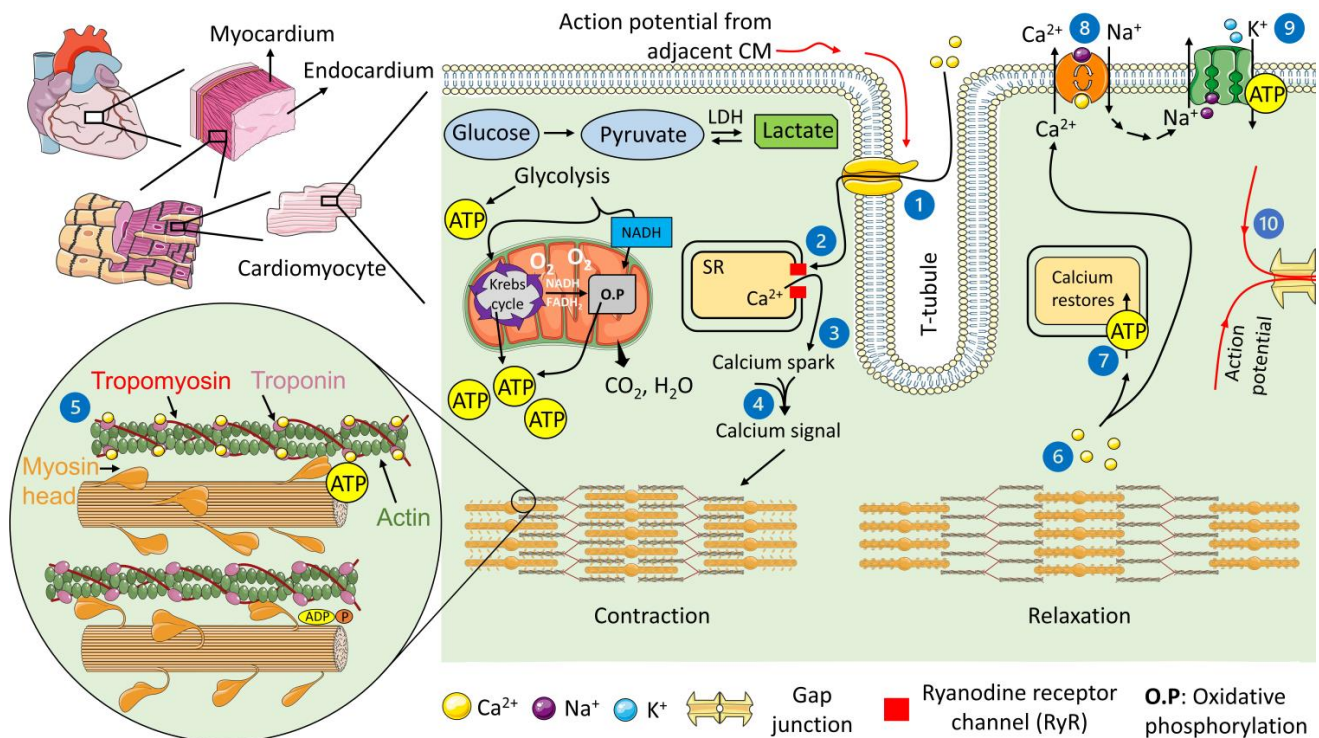


Figure 3. Contractile machinery of the heart: (1) Voltage-gated calcium channels open. Influx of Ca^{2+} ions. (2) Calcium-induced calcium release through RyR receptor channel. (3) Local release causes calcium spark. (4) All sparks sum up to create calcium signal. (5) Ca^{2+} binds to troponin to initiate contraction. (6) Upon relaxation, Ca^{2+} unbinds from troponin. (7) Ca^{2+} is pumped backed to sarcoplasmic reticulum (SR). (8) Ca^{2+} and Na^+ are exchanged with each other through exchangers. (9) Na^+ gradient is maintained through sodium-potassium pump. (10) The action potential travels to the adjacent CM through the gap junction.

3. The Damage to the Contractile Machinery due to Ischaemia

Blood provides the heart with glucose, oxygen, and other nutrients to make ATP. Any delay in the blood supply would lead to a deficiency of these vital nutrients and perturbations in the intracellular processes. Since the heart requires a smooth supply of blood for its perpetual function, this gap in supply and demand also referred to as “ischaemia” triggers a chain of anomalies. During normoxia, about 90% of the total ATP is produced via the oxidative phosphorylation process in the mitochondria while anaerobic glycolysis only makes up 5–10% of total ATP. Sudden cessation of the oxidative phosphorylation process due to ischaemia initiates the systolic dysfunction, and CMs must find alternative ATP sources. High-energy creatine phosphate could fuel the process for a while, but their supply is exhausted quickly [16] and anaerobic glycolysis becomes the main source of creating new ATP and results in the rapid accumulation of lactate in the form of lactic

acid leading to intracellular acidosis. Inorganic phosphate generated from the breakdown of creatine phosphate and acidosis leads to the inefficient binding of calcium ions to the contractile proteins. Since no glucose is supplied to the cardiomyocytes through blood, the main supply of glucose for cytosolic glycolysis comes from the stored intracellular glycogen stockpiles. Even at its fastest rate, anaerobic glycolysis cannot replace a much more efficient oxidative phosphorylation process. As a result, ATP is consumed more quickly than it is produced. Intracellular acidosis due to the gradual accumulation of lactate blocks many of the enzymes of the glycolytic pathways. Therefore, several minutes after ischaemia the rate of anaerobic glycolysis is considerably suppressed until it stops altogether even if the glycogen reserves are present to feed the process [17]. This marked drop in ATP amounts in the ischaemic myocardium leads to irreversible changes in the CMs because the energy-depleted cells cannot maintain their homeostasis.

The severe downfall of the metabolic activities in ischaemic CMs also leads to marked perturbations in the intracellular ionic levels [18]. Ischaemic cells secrete out K^+ in the interstitial matrix [19], and the gradual accumulation of extracellular K^+ results in inexcitability and the conduction block. In the ischaemic area, the increased production and inefficient removal of protons (H^+) result in acidosis as pH falls by one unit or more. This intra- and extracellular acidosis block many ionic channels leading to a fall or prolongation of the action potentials with the creation of early depolarisations [20]. The dysfunction of the sodium-potassium pump and sodium-calcium exchanger results in the intracellular overload of Na^+ and Ca^{2+} levels that creates an arrhythmogenic environment. Mg^{2+} bound to ATP is also released from the hydrolysed ATP in the ischaemic area. This chain of events seriously compromises the electrophysiological functions of the ischaemic myocardium which would lead to total heart failure in the long run.

4. The Scar Formation and Its Electrophysiological Remodelling

As prolonged ischaemia causes irreversible damage to the cardiomyocytes it also wrecks the cardiac extracellular matrix. In the following days and months, ischaemic tissue undergoes a healing process, and the lost contractile tissue is replaced by collagen-rich fibrotic scar tissue. This scar tissue offers some degree of compliance during active pumping and prevents the heart wall from rupturing. However, its inability to conduct electric currents induces lethal arrhythmias and asynchronous beating resulting in ventricular dysfunction that ultimately leads to total heart failure. Soon after the MI, the infarction site is infiltrated by macrophages and neutrophils. They release inflammatory mediators, such as matrix metalloproteinases (MMPs) and tumour necrosis factor (TNF) that remove dead cells and disintegrated ECM debris. Four days post-MI, a pink granulation tissue starts to form on the ischaemic area, and it consists of myofibroblasts, inflammatory cells, and new blood vessels to restore the blood supply. Myofibroblast is the activated state of cardiac fibroblast which secretes out excessive collagen at the site of injury. They are not present in the healthy myocardium and the infarction area; they replace the dead cardiomyocytes as they demonstrate some degree of contractility. This granulation tissue rich in collagen eventually turns into scar tissue devoid of inflammatory cells but rich in ECM and myofibroblasts [21]. Since the heart cannot pump efficiently due to the loss of cardiomyocytes during the scar maturation process, the heart slowly starts to dilate resulting in ventricular remodelling and total heart failure in the long run [22].

Gap junctions (GJs) mediate the propagation of electric signals throughout the myocardium, and they are located at intercalated discs (ID) between adjacent cardiomyocytes. They are comprised of connexin protein; the most common of which is connexin 43 (Cx43) in mammalian hearts [23]. Due to infarction, not only does the GJs density decrease but Cx43 tends to reorganise itself away from the ID zone as shown in Figure 4. Decreased electrical activity in the ischaemic area is correlated to the dephosphorylation and translocation of Cx43 from ID to non-ID sites [24,25]. This translocation of GJs interrupts normal electrical conduction of the heart and could lead to arrhythmias [22,26–28]. At the boundary of the infarct lies a few cells' thick transitional areas referred to as the infarct border zone (IBZ)

that lies between the ischaemic tissue and the viable myocardium. The inefficient removal of the toxic biochemical products, Cx43 translocation, cellular organisation, and collagen deposition all could lead to the generation of arrhythmias in the IBZ [29–31]. Surviving cardiomyocytes in the IBZ have reduced Na^+ levels [32,33] and the repolarising K^+ currents lead to a prolonged duration of action potentials [34,35]. These consequences along with the perturbation in the intracellular calcium levels result in decreased excitability and altered resting membrane potential [36]. Inefficient performance of sodium-calcium exchanger due to ischaemia may lead to a marked reduction in the expression of sarcoplasmic reticulum calcium ATPase (SERCA) that regulates the flow of Ca^{2+} from the cytosol to the sarcoplasmic reticulum. This leads to irregular intracellular Ca^{2+} levels that result in delayed action potentials, arrhythmias, and LV dysfunction [37–39].

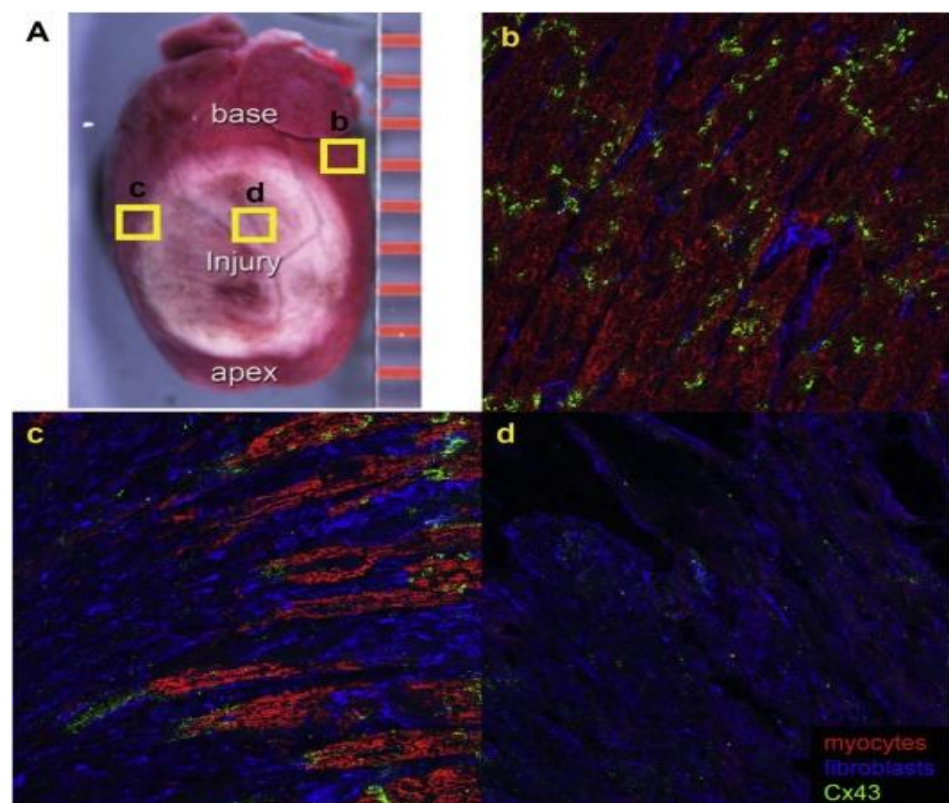


Figure 4. Structural changes in healed infarct scar. (A) The scar differentiates in the ischemic portion of the heart. (b) Cx 43 (green) is localised to the IDs in remote myocardium. (c) Fibroblasts (blue) interrupt normal myocyte (red) connections in the IBZ adjacent to the scar and Cx 43 reorganises away from the IDs. Cx 43 is often found between myocytes and fibroblasts. (d) Punctate Cx 43 is found within the scar. Reprinted with permission from [36]. Elsevier, all rights reserved.

5. Hostile Microenvironment of the Injured Myocardium and the Post-MI Remodelling

After an ischaemic attack, the microenvironment of the myocardium becomes hostile to cells due to the inflammatory response. This is the body's natural response to repair the injury and it involves complex biochemical processes; the result of which is scar formation. The complete biochemical explanation of this hostile microenvironment including the factors involved, their roles, biological pathways etc. is given elsewhere [40,41]. In a nutshell, there are three main factors responsible for this hostile microenvironment: (i) generation of free radicals due to ischaemia, (ii) migration of the leukocytes to the injury site in response to chemokine expression, and (iii) secretion of pro-inflammatory cytokines by injured cardiomyocytes and the migrated leukocytes, as shown in Figure 5 [42]. This inflammatory microenvironment is the principal culprit of why certain therapeutic approaches, such as

stem cell therapy and tissue engineering methods, fail in the first place. A better understanding of this stressful condition could help us develop practical approaches to address the problem.

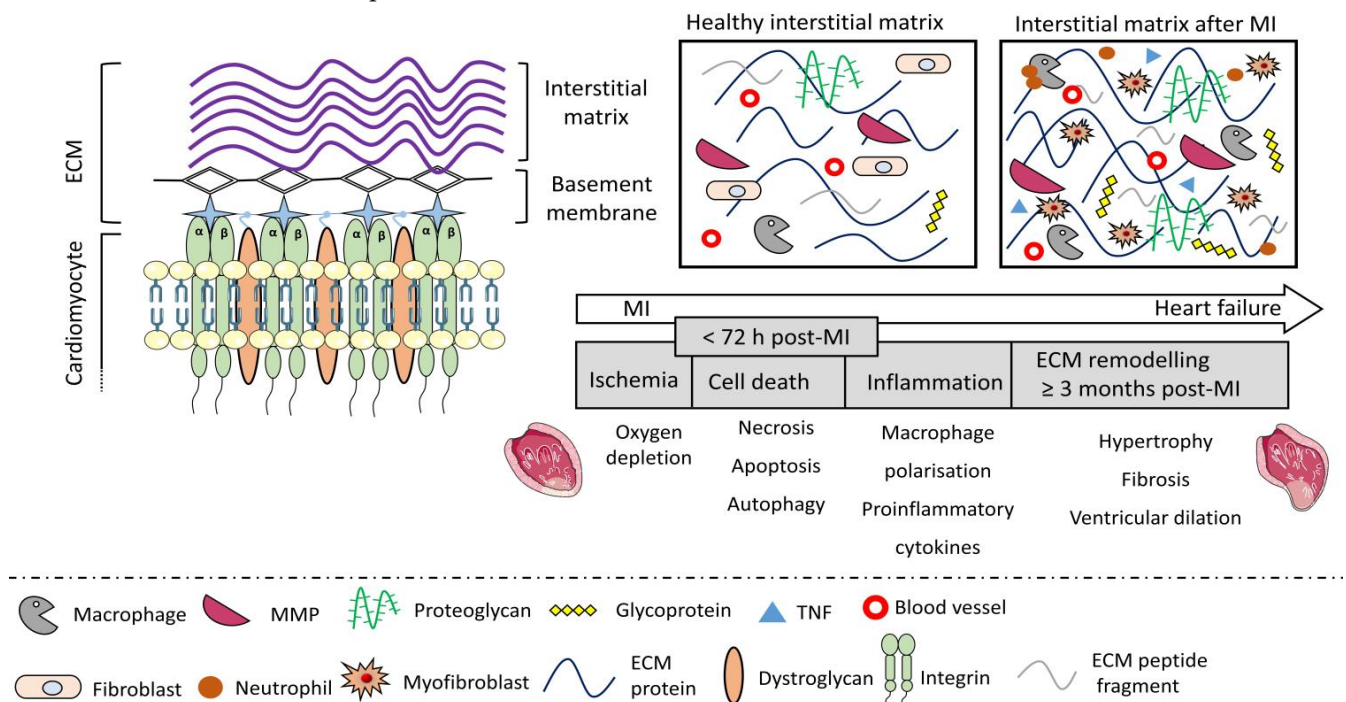


Figure 5. ECM components: Interstitial matrix consists of fibrillar collagen, elastin, proteoglycans, and glycoproteins; basement membrane is made of non-fibrillar collagen and laminin. Cardiomyocytes attach to the basement membrane via transmembrane proteins, such as integrin and dystroglycan. The excessive ECM secretion after the infarction leads to tissue hypertrophy and scar formation preventing quick ventricular dilation and tissue rupture. Adapted from [14] under the CC-BY license.

Shortly after an infarction, free radicals are produced in the cytoplasm of ischaemic cardiomyocytes via mitochondrial pathways. These free radicals which are also referred to as reactive oxygen/nitrogen species trigger the chemotactic infiltration of inflammatory cytokines, such as macrophages, neutrophils, tumour necrosis factor (TNF), and matrix metalloproteinases (MMPs). Macrophages/neutrophils remove dead cell/tissue debris, while MMPs break down the ECM structure [43]. In addition to apoptosis, these pro-inflammatory cascades also convert cardiac fibroblasts into more activated myofibroblasts to secrete out excessive ECM components. As a result, scar tissue rich in collagen is formed to replace the lost myocardial tissue and to prevent tissue rupture due to perpetual heart contraction. In the long run, this scar tissue induces arrhythmias due to the inability of inert collagen to conduct electric currents thus deteriorating and failing the heart.

6. How Has T.E Helped So Far to Mitigate the Problem?

Cardiac tissue engineering has emerged as a promising solution to address the issue. By engineering, heart-like tissues researchers were able to replace the injured myocardium with artificial tissue in animal models [44,45]. A cardiac patch made of gelatin methacryloyl (GelMA) cultured with hiPSCs-derived cardiomyocytes, smooth muscle cells, and endothelial cells was engrafted onto a murine MI model. Four weeks post-implantation, cardiac functions improved. However, cell engraftment decreased from 24.5% at week 1 to 11.2% at week 4 [46]. Human-embryonic-stem-cells-derived cardiomyocytes (hESCs-CMs) survived for two weeks in the nude rat myocardium when cultured on a poly(hydroxyethyl methacrylate)-co-methacrylic acid scaffold. The small pore size (30–40 μm) of the scaffold led to angiogenesis at the infarction site with reduced M2 macrophage levels [47]. Likewise, a fibrin-based cardiac patch, when cultured with CMs, improved the cardiac function and

remodelling of the deteriorating myocardium in the rats after an MI [48]. Four weeks after subcutaneous implant in the rats, infiltration of endogenous cells and vascularisation was observed in acellular cardiac ECM/silk patches. While an elastomeric polyglycerol sebacate patch provided mechanical compatibility to the myocardium and reduced the hypertrophy, it could not support the systolic function of the failing myocardium [49,50]. Mouse-embryonic-stem-cells-derived cardiomyocytes (mESCs-CMs) integrated well with the host myocardium when injected with nano-matrix gels containing RGDS motifs. One week after injection at the injury site about 90% of CMs survived which led to improved cardiac functions that sustained for twelve weeks [51]. In vivo efficacy of different biomaterials, cell types, and the therapeutic potential of cardiac tissue engineering to treat infarcted myocardium, including pre-clinical and clinical studies, has been extensively reviewed [12].

Stem cell therapy has faced the serious challenge of cell engraftment in the hostile environment following myocardial infarction. Some degree of success has been achieved via a tissue engineering approach by engrafting cells with biomaterials and growth factors at the injury site. However, the benefits observed in the clinical studies have been less consistent mainly due to the poor integration of the transplanted cells/biomaterial with the host myocardium. The conventional tissue engineering approach using a non-conductive scaffold cultured with cells and then implanted in-vivo has not been quite as helpful in improving the electrophysiological functions of the failing heart. In the presence of already inert scar tissue, the implantation of the non-conductive construct could make matters worse by generating arrhythmias and will not be able to restore the electrophysiological functions of the injured heart. To tackle this issue, one possibility could be the implantation of a conductive construct matching the electrical properties of the myocardium. This way the scar tissue, which acts as a blockage to the propagation of action potentials across the heart, could be overcome with a conductive construct, and a steady flow of electrical signals could be restored as shown in Figure 6.

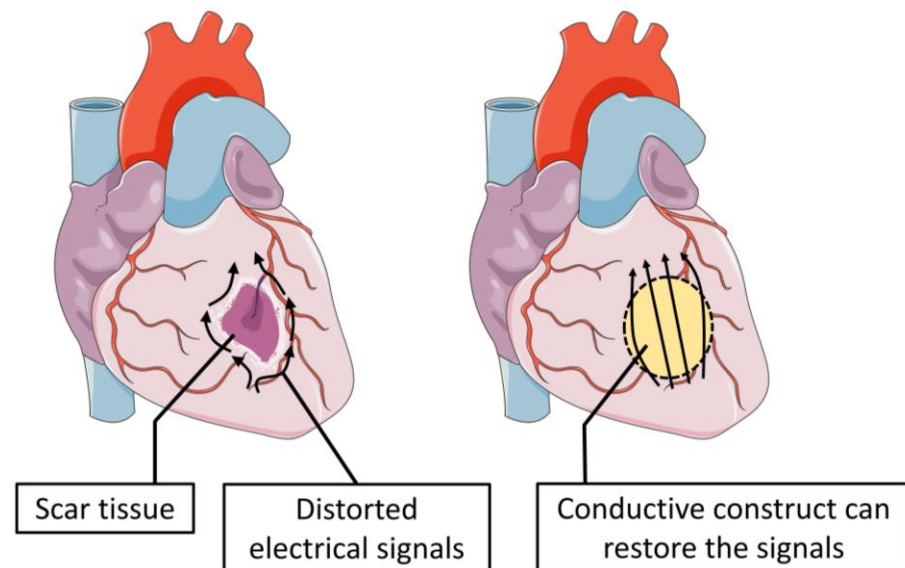


Figure 6. Electrical signals blocked by the scar tissue after an infarction. A conductive construct can restore the signal transmission through it.

7. The Conductive Scaffold

Several carbon-based conductive nanomaterials (carbon nanotubes, graphene, metallic nanoparticles, etc.) could be blended with natural or synthetic biomaterials to fabricate a conductive construct. With this approach, the differentiation potential of cardiac, nerve, and muscle cells could be increased several-fold as these cells are more electrically responsive. Besides providing a biocompatible microenvironment, the conductive scaffold can also improve the intercellular propagation of electrical signals. With a balanced interplay between physicochemical and electrical cues, cells can attain mature native-like phenotype.

7.1. Carbon Nanotubes

The excellent electrical conductivity of carbon nanotubes (CNTs) has put them in the limelight of a conductive scaffold-based tissue engineering approach. Single wall carbon nanotubes (SWCNTs) embedded with collagen composites triggered the β 1 integrin-mediated pathways in the cultured neonatal rat ventricular myocytes (NRVMs). These pathways led to the formation of junctional proteins that ultimately resulted in the improved assembly of intercalated discs in the matured cells [52]. Likewise, CNTs embedded with polyurethane/chitosan conductive membranes significantly improved the viability of H9c2 cells one week post-culture [53]. In addition to their positive contributions, SWCNTs could pose complications due to their small size (1–3 nm diameter) by penetrating the plasma membrane and disrupting the intracellular processes in the long run [54–57]. To avoid this, carbon nanotubes are often used as multi-wall carbon nanotubes (MWCNTs) with a diameter ranging from 10–200 nm. The positive effect of MWCNTs was observed when blended with a decellularised pericardium extracellular matrix. One week post-culture, the proliferation rate of HL-1 myocytes increased three-fold with enhanced expression of Cx43 and α -actinin [58].

A continuous electrical stimulation (1 Hz, 8 V, 10 ms pulses) was applied to C2C12 myoblasts cultured on gelatin methacryloyl/MWCNTs hydrogels. The cell manifested a strong cardiomyocyte-like phenotype evident when the expression of MRF4, MHC, myogenin, and α -actinin upregulated several-fold [59]. Carbon nanotubes have also been proven to shift the differentiation of various stem cell lines towards myocardial differentiation. This was observed when unrestricted somatic stem cells generated cardiomyocyte-like cells when cultured on MWCNTs-embedded biomaterials. Differentiated cells demonstrated a heart-like contractile phenotype as shown by the enhanced levels of Cx43, cTnI, and β -MHC when electrically stimulated compared with when cultured on non-conductive scaffolds [60]. Similarly, 129/SVE-derived mouse stem cells generated embryoid bodies (EBs), which could be thought of as a 3D bundle of stem cells, when cultured on gelatin methacrylate/CNT hydrogels. EBs started to beat with 1.8 beats per second when stimulated electrically compared with when cultured on non-conductive hydrogels. An exceptional increase in the expression of cardiac-specific genes, such as Nkx2.5 (14.8-fold), Myh7 (4.9-fold), cTnT2 (59.6-fold), and Tbx5 (3.9-fold), was observed when CNTs were embedded inside of these EBs. However, embryonic bodies without CNTs did not show a well-pronounced cardiac phenotype [61,62].

CNTs embedded silk and gelatin methacrylated (GelMA) conductive patches significantly improved the cell maturation when cultured with neonatal rat cardiomyocytes. Seven days later, cultured cells demonstrated elevated expression of α -actinin, Cx43, and cTnT with synchronous beating patterns compared with when cultured on non-conductive patches, particularly when electrically stimulated [63,64]. Similarly, SWCNTs embedded in collagen hydrogel resulted in the formation of engineered cardiac tissue with strong contraction potential when cultured with cardiomyocytes [65]. While MWCNTs blended with polycaprolactone (PCL), and polyethylene glycol improved the viability and proliferation of rat myoblasts seven days post-culture when coated with fibrin glue [66].

Pristine carbon nanotubes have also been used as a platform to enhance the electrical coupling and contractility among cultured cells. Pristine carbon nanotube films were cultured with neonatal rat ventricular myocytes and cardiac fibroblasts. Cells developed tight desmosomes-like nano connections and started to beat rhythmically compared with when cultured on non-conductive constructs [67,68]. Table 1 shows some practical applications of carbon nanotubes in tissue engineering.

Table 1. Carbon nanotubes-based conductive constructs for cardiac tissue engineering applications.

| Conductive Construct | Mechano-Electrical Properties | Electrical Stimulation | Cell Line | Cellular Behaviour |
|--|---|--|----------------------------------|---|
| Collagen/SWCNTs composite [52] | $\sigma = 1.72 \times 10^{-9} / \Omega$ | - | NRVMs | Enhanced assembly of intercalated discs |
| PU/chitosan/CNTs membranes [53] | UTS = 21.9 MPa, E = 4.34 MPa, R = 0.17 k Ω /sq | - | HUVECs, H9c2 | Improved cell viability |
| Decellularised pericardium ECM, MWCNTs hydrogels [58] | G' = 229 Pa, G'' = 150 Pa, $\sigma = 15 \times 10^{-3}$ S/cm | - | HL-1 | Three-fold increase in the proliferation rate |
| MWCNTs, GelMA hydrogels [59] | E = 23.4 kPa, Z = 400 k Ω | 10 ms AC pulses at 1 Hz and 8 V for 2 days | C2C12 | Myotube formation when stimulated electrically |
| CHI, PVA, MWCNTs membranes [60] | E = 941 MPa, $\epsilon_r = 3.8\%$, $\sigma = 1.2$ mS/cm | Monophasic pulses at 1.25 Hz and 10 V for 2 days | USSCs | Differentiation to cardiomyocyte-like cells |
| GelMA-CNTs hydrogels [61] | E = 30.6 kPa, Z = 56 k Ω at 0.2 Hz | 10 ms AC pulses at 1 Hz and 3V for 2 days | 129/SVE-derived mouse stem cells | Formation of beating embryoid bodies with enhanced expression of cTnT2 and Nkx2.5 |
| CNTs embedded inside of EBs [62] | E = 35.2 kPa, Z = 300 k Ω at 1 Hz | 10 ms AC pulses at 1 Hz and 3V for 2 days | 129/SVE-derived mouse stem cells | Several fold increase in the expression of Nkx2.5, acta2, cTnT2, MHC, MLC, and Cdh5 genes |
| Silk/CNTs patch [63] | E = 51 kPa, $\epsilon_r = 42\%$, R = 94 k Ω | AC square waveform at 1 Hz | neonatal rat CMs | Synchronous beating patterns with contractile phenotype |
| GelMA/CNTs patch [64] | E = 32 kPa, Z = 2 k Ω at 1000 Hz | AC 50 ms pulses between 0.5–3 Hz at 1 V/cm | neonatal rat CMs | Three times higher spontaneous contractions than GelMA |
| SWCNTs/collagen hydrogel [65] | Mechanical strength = 24 kPa, $\sigma = 525$ mS/m | - | CMs | Formation of engineered cardiac tissue with strong contraction potential |
| MWCNTs/PCL/PEG/fibrin glue patch [66] | E = 47 MPa, $\sigma = 0.45$ S/m | - | Rat myoblasts | Improved cell viability and proliferation |
| Pristine CNTs films [67] | $\sigma = 3.1$ mS | 2 ms AC pulses at 1 Hz and 2 V/cm for 3 days | neonatal rat CMs | Synchronous beating patterns after stimulation |
| Pristine MWCNT films [68] | - | - | NRVMs, cardiac fibroblasts | Development of striated morphology with tight desmosomes like nano-connections |
| PGS-gelatin/CNTs membranes [69] | E = 373 kPa, Z = 7 k Ω at 40 Hz | 50 ms AC biphasic pulses, V = 0–7 volts, f = 1–3 Hz | Neonatal rat CMs | Twice the beating rate five days post-culture on the conductive membranes |

7.2. Graphene

With its exceptional electrical properties in 2D, graphene and its derivatives are promising candidates for regenerating electrically active biological tissues (Table 2). Reduced graphene oxide (rGO) foam led to the maturation of cultured neonatal rat CMs. Ten days post-culture, cells organised themselves ubiquitously throughout the porous foam. Different cell clusters in various locations in the conductive foam started to protrude branches that merged forming a large beating syncytium with 65 beats per minute [70]. Graphene-based constructs also influence the differentiation of adult stem cells. Human-bone-marrow-derived mesenchymal stem cells readily differentiated into cardiomyocyte-like cells when cultured on rGO/alginate hydrogels. Differentiated cells demonstrated good viability with a strong CM-like phenotype [71]. Graphene oxide blended with different biomaterials improved the cell morphology of the cultured CMs and neonatal rat cardiac fibroblasts. Cells developed spatial cytoskeletal morphology with striated sarcomeres evident from the enhanced expression of α -tubulin, Cx43, cTnT2, and intercalated discs related proteins, such as N-cadherin [72,73]. Improved intercellular coupling among the cultured cells was observed that ultimately led to the synchronous beating of CMs. A conductive graphene patch generated synchronous beating CMs matured from mESCs-CMs [74]. GelMA/rGO cultured CMs demonstrated nine times faster beating rate compared with when cultured on non-conductive GelMA hydrogels [75].

Table 2. Graphene based conductive constructs for cardiac tissue engineering applications.

| Conductive Construct | Mechano-Electrical Properties | Electrical Stimulation | Cell Line | Cellular Behaviour |
|---------------------------------------|--|---|-------------------------------------|--|
| rGO foams [70] | $G' = 8 \text{ kPa}$, $\sigma = 112 \text{ S/m}$ | - | Neonatal rat CMs | A 3D cellular organisation within conductive foam that formed a large beating syncytium with 65 bpm |
| rGO/alginate hydrogels [71] | $G' = 1 \text{ kPa}$, $\sigma = 1/9 \pm 0.16 \times 10^5 \text{ S/m}$ | - | hBM-MSCs | Differentiation to CMs-like cells |
| rGO/collagen patch [72] | $E = 340 \text{ kPa}$, $\sigma = 22 \mu\text{S/m}$ | - | CMs | Elevated expression of Cx43 and cTnT2 |
| OPF/GO hydrogels [73] | $\sigma = 4.24 \text{ mS/cm}$ | - | Neonatal rat cardiac fibroblasts | Well-organised sarcomeres with enhanced expression of α -tubulin, and actinin |
| PCL/CHI/PPy/graphene patch [74] | $E = 0.098 \text{ MPa}$, $\text{UTS} = 1.27 \text{ MPa}$, $\epsilon_r = 8\%$, $\sigma = 5.33 \text{ S/cm}$ | - | mESCs-CMs | Elevated troponin levels with beating CMs |
| GelMA/rGO hydrogels [75] | $E = 22.6 \text{ kPa}$, $Z = 1.5 \text{ k}\Omega$ at 100 Hz | 50 ms AC biphasic pulses at 1–3 Hz and 3–6 V/cm | Primary CMs | Nine times faster beating rate compared to when encapsulated in non-conductive hydrogel |
| rGO/dECM hydrogels [76] | $E = 17.5 \text{ kPa}$, $\sigma = 3 \text{ S/m}$ | - | hiPSCs-CMs and HS-27A stromal cells | Generation of engineered heart tissue with elevated expression of voltage-gated calcium and potassium channels |
| PCL, graphene composites [77] | $\sigma = 1.5 \times 10^{-8} \text{ S/m}$ | 10 ms AC pulses at 1 Hz and 5 V | mESC-CMs | Average beating frequency 1.1 beats/second two weeks post-culture |
| Chitosan/GO-Au patch [78] | $\sigma = 12 \times 10^{-5} \text{ S/cm}$ | - | hiPSCs-CMs | Improved cell adhesion |
| rGO/GelMA/polydopamine hydrogels [79] | $E = 23.6 \text{ kPa}$, $Z = 1250 \Omega$ at 1000 Hz | AC 2 ms triphasic pulses at 1.5 Hz | CMs | Improved calcium transients with 40 bpm |
| rGO/silk electrospun membranes [80] | Tensile strength = 6 MPa, $\sigma = 0.3 \text{ S/cm}$ | AC 5 ms square wave pulses at 100 Hz | CMs and myofibroblasts | Improved cell viability. However, the stimulation caused ventricular fibrillation |

7.3. Fullerene

Fullerene is a zero-dimensional allotrope of carbon and the most famous of all is the hollow ball of 60 carbon atoms also known as buckminsterfullerene (C-60 fullerene). Fullerene and its derivatives have been candidates of interest for various biomedical applications [81]. In one of the studies, C-60 fullerene particles were suspended in a cell suspension containing brown adipose-derived stem cells (BADSCs). After seven days, fullerenes modulated cardiomyogenic differentiation by improving MAPK expressions in BADSCs. This also led to improved cell survival, proliferation, and cardiomyogenesis evident from the enhanced expression of cTnT2 and α -actinin compared with the cell suspension without fullerenes [82]. Quite often the hydrophobic nature of C-60 fullerene in its pristine form limits its ability to fabricate a scaffold or construct. Therefore, it is usually conjugated with -OH groups on the surface to make it water soluble, referred to as “fullerenol”. An injectable fullerenol/alginate-conductive hydrogel was able to suppress the oxidative stress damage in the cultured BADSCs in the presence of hydrogen peroxide. These conductive hydrogels improved the survival capability of the cells under this oxidative stress microenvironment by activating ERK/p38 and inhibiting JNK pathways. Under these favourable conditions, cells differentiated into cardiomyocyte-like cells and expressed a striated contractile morphology [83]. C2C12 myoblasts generated multi-nucleated myotubes when cultured on highly directional one-dimensional fullerene whiskers. Compared with the random formation of the myotubes on the glass control, cells proliferated, along the whisker’s length, generating aligned myotubes with high fusion/maturation indices and elevated expressions of MyoD and myogenin [84]. Table 3 shows some applications of fullerenes for cardiac tissue engineering.

Table 3. Fullerene-based conductive constructs for cardiac tissue engineering applications.

| Conductive Construct | Mechano-Electrical Properties | Electrical Stimulation | Cell Line | Cellular Behaviour |
|---|----------------------------------|------------------------|-----------|---|
| Cell suspension + C-60 fullerene NPs [82] | - | - | BADSCs | Improved MAPK expression led to the differentiation of BADSCs to cardiomyocyte-like cells |
| Fullerenol/alginate hydrogels [83] | $G' = 700$ Pa, $G'' = 100$ Pa | - | BADSCs | Inhibition of ROS environment by activating ERK/p38 pathways which led to better cell survival and cardiomyogenic differentiation |
| Fullerene whiskers [84] | - | - | C2C12 | Myogenic differentiation with elevated expression of MyoD and myogenin |

7.4. Carbon Nanofibers

Carbon nanofibers (CNFs), just like CNTs, can also be reinforced into inert biomaterials to develop conductive constructs. In one of the studies, CNFs were embedded in collagen extracted from rat tail tendon, and the gels were lyophilised to fabricate conductive nanocomposites. Cultured H9c2 cells demonstrated good viability with a pronounced expression of contractile α -actinin protein [85]. Cardiomyocytes cultured on a gelatine/CNF conductive patch exhibited mature sarcomeric morphology with elevated gap junction proteins compared with when cultured on non-conductive gelatine constructs [86]. Likewise, CNF/chitosan composites improved the intercellular electrical coupling in cultured neonatal rat CMs. This coupling led to a mature cardiomyocyte-like phenotype evident from enhanced expression of Cx43, myosin heavy chain protein (MHC), atrial natriuretic factor (ANF), and troponins. ANF is a hormone secreted by the cardiomyocytes during

wall stretching, and it maintains circulatory homeostasis [87,88]. Table 4 reports some practical applications of carbon nanofibers in cardiac tissue engineering.

Table 4. Carbon nanofibers-based conductive constructs for cardiac tissue engineering applications.

| Conductive Construct | Mechano-Electrical Properties | Electrical Stimulation | Cell Line | Cellular Behaviour |
|------------------------------|---|------------------------|------------------|--|
| Collagen/CNF composites [85] | Mechanical strength = 3.5 N | - | H9c2 | Elevated expression of α -actinin |
| Gelatin/CNF patch [86] | E = 8.42 MPa, UTS = 5.32 MPa, $\sigma = 84 \mu\text{S/m}$ | - | CMs | Three- to four-fold increase in actn4 and Cx43 expression. |
| Chitosan/CNF composites [87] | E = 28 kPa, $\sigma = 0.25 \text{ S/m}$ | - | Neonatal rat CMs | Cell maturation with contractile phenotype evident from elevated expression of cyto-skeletal Cx43, GATA4, troponins, Myh6, Myh7, and ANF |
| PLA/CNFs membranes [89] | E = 389 kPa, $\sigma = 0.58 \text{ S/m}$ | - | Neonatal rat CMs | Elevated expression of α -actinin, Cx43 and β -actin |
| PLGA/CNFs composites [90] | E = 7.9 MPa, $\sigma = 0.1 \text{ S/m}$ | - | CMs | Increased cell growth and density five days post-culture |

8. Possible Cell-Matrix Interactions

The cellular behaviour of the cells cultured on a conductive scaffold is different compared with the cells cultured on a non-conductive scaffold. As explained in the above section, the voltage-gated ion channels could be opened by electronic currents travelling through the conductive scaffold. These channels could also be opened via electrical stimulation [91]. This leads to a disturbance in the ionic concentration across the plasma membrane, and an influx of ions (Na^+ , K^+ , Ca^{2+}) takes place through these opened channels causing membrane depolarisation. In the cytoplasm, the calcium-binding protein calmodulin is activated by binding to Ca^{2+} ions which in turn activates calcineurin by dephosphorylating it [92]. MAPK/ERK signals generated by the interaction between integrin and scaffold strands together with signals generated by phosphorylated NFAT trigger an intracellular cascade of pathways. These pathways may lead to the expression of cardiac-specific genes, such as Nkx2.5, GATA4, Cx43, etc. when cultured with cardiac stem cells [93–95]. The expression of such genes indicates the differentiation of cardiac stem cells to cardiomyocyte-like cells with contractile phenotype. GATA4 and Nkx2.5 are cardiac-specific transcription factors that play a fundamental role in myocardial differentiation in the early stages of cardiogenesis in a developing embryo. Troponin proteins that play an important role in heart contractility are expressed in the heart muscles of mammalian and avian species [96–98]. Connexin 43 (CX43) is the principal gap junction protein of the heart that facilitates the transmission of action potentials from cell-to-cell to synchronise the beating [99]. The expression of cytoskeletal structural proteins, such as myosin heavy chain (MHC), myosin light chain (MLC), and α -actinin, indicate that the cultured cells have developed a contractile cardiomyocyte-like phenotype and are now fully differentiated. Figure 7 demonstrates a scheme of these cell-matrix interactions. The following sections will shed light on how conductive constructs assist stem cells to develop an in-vivo-like tissue phenotype.

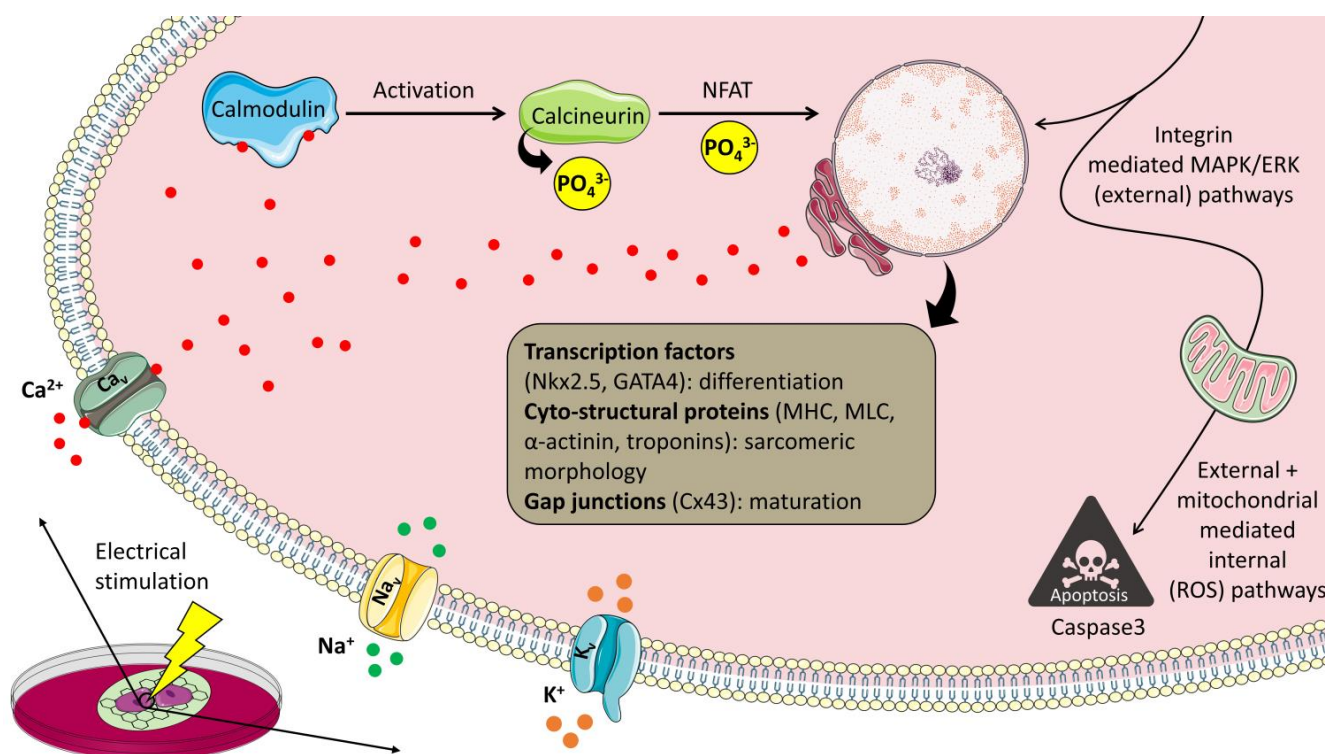


Figure 7. A scheme of cardiac stem cells cultured on a graphene-based conductive construct. This construct can trigger intracellular signalling pathways particularly when electrically stimulated. Such pathways can lead to the expression of cardiac specific genes that are an indication of the cardiac-like phenotype of the cultured cells. Sometime harmful external pathways (contamination of the culture medium due to high concentration of cell metabolic waste, extreme stiffness of the scaffold and toxicity of CNMs etc.) along with internal mitochondrial pathways (reactive oxygen species) can result in cell death via apoptosis by activating caspase genes.

9. In Vivo Efficacy of the Conductive Constructs

In an attempt to control the cardiomyogenic differentiation potential of various stem cell lines, the conductive scaffold-based tissue engineering approach is a leap forward. It provides platforms through which cultured cells can achieve cardiomyocyte-like phenotype. However, the fabrication of such platforms/constructs mimicking the ECM microenvironment to encourage appropriate cell-cell and cell-matrix interactions is arduous. An optimum construct should be biocompatible with suitable porosity to deliver biological factors and remove metabolic waste. Furthermore, it must provide appropriate mechano-structural cues in the form of stiffness, and micro/nano topography, possessing suitable electrical conductivity to provide the cultured cells with an in-vivo-like electrophysiological microenvironment. Such cell-free or cell-laden constructs should also be able to integrate well with the host tissue when implanted in vivo without inducing any tissue inflammation or immune response. Taken together, when all these criteria are met a niche or cradle is generated in which the cell-cell coupling or pathways among the cultured stem cells would be in perfect harmony, just like it exists among the cells inside the body. Studies on animals (Table 5) have shown that electroconductive constructs have substantially alleviated various functions of the infarcted heart when implanted at the injury site.

Table 5. In vivo efficacy of CNMs-based conductive scaffolds to repair the ischaemic heart tissue in rats.

| Conductive Construct | Injured Heart | Implanted Heart |
|---------------------------------------|---|---|
| OPF/GO hydrogels [73] | Wall thickness = 0.37 mm | Wall thickness = 0.77 mm |
| Chitosan/GO-Au patch [78] | Ejection fraction = 40% Fraction shortening = 19% | Ejection fraction = 70% Fraction shortening = 40%, Shorter QRS interval |
| rGO/silk electrospun membranes [80] | Ejection fraction = 46% Fraction shortening = 23% Wall thickness = 0.7 mm | Ejection fraction = 68% Fraction shortening = 38% Wall thickness = 1.2 mm |
| Fullerenol/alginate hydrogels [83] | Wall thickness = 0.61 mm | Wall thickness = 1.3 mm |
| Collagen/CNFs composites [85] | High tissue degeneration with the damaged assembly of intercalated discs | Improved angiogenesis with the repair of intercalated discs assembly |
| PLA/CNFs membranes [89] | Ejection fraction = 50% Fraction shortening = 29% Wall thickness = 0.8 mm | Ejection fraction = 75% Fraction shortening = 45% Wall thickness = 2.4 mm |
| Gelatin/SWCNTs hydrogels [100] | Ejection fraction = 43% Fraction shortening = 19% | Ejection fraction = 49% Fraction shortening = 29% |
| PNIAA/SWCNTs hydrogels + BADSCs [101] | Wall thickness = 538 μ m | Wall thickness = 863 μ m |
| PEG-MEL/HA-SH/GO composites [102] | Wall thickness = 0.9 mm | Wall thickness = 1.9 mm |
| SF, GO hydrogels [103] | Wall thickness = 250 μ m | Wall thickness = 280 μ m |

Carbon nanomaterials have also demonstrated good in vivo efficacy when it comes to restoring the cardiac functions of the injured heart. Cardiac tissues are engineered by culturing neonatal rat cardiac cells on gelatine/single-wall carbon nanotube hydrogels integrated well with the host myocardium. Four weeks post-implantation, CMs infiltrated the scar tissue and exhibited cTnT, actinin, and Cx43 expressions, which are an indication of good integration of these CMs into the scar tissue. Injured hearts that received these engineered tissues also demonstrated good blood pumping ability compared with the hearts that did not receive any such treatment [100]. Brown adipose-derived stem cells (BADSCs) survived the hostile microenvironment of the infarcted tissue when injected with poly(N-isopropylacrylamide)/SWCNTs conductive gels. Four weeks post-injection, LV wall thickness increased to 863 μ m compared with 538 μ m in the case of infarcted hearts [101].

Similarly, graphene oxide (GO), when blended with different biomaterials, improved various heart functions after implantation. Improved tissue regeneration was observed with an LV wall thickness of 1.9 mm compared with 0.9 mm in MI hearts after four weeks of implantation [102]. Infarct size was reduced by 1.8-fold with improved blood pumping ability and reduced the left ventricle diameter at end-systole and end-diastole [73,103]. Injured hearts injected with fullerenol/alginate hydrogels with BADSCs demonstrated improved angiogenesis with twice the vessel density and LV wall thickness compared with when the hearts were injected with PBS and BADSCs only [83]. Collagen/carbon nanofiber composites repaired the damaged intercalated discs assembly. A sarcomeric phenotype was observed in the regenerated tissue with high angiogenesis [85].

10. Drawbacks

Even though carbon nanomaterials-based conductive scaffolds have demonstrated useful potential to address the ischaemic heart tissue problem, carbon nanomaterials themselves could pose serious health complications. Of several such complications, the destruction of cellular structure, inflammation, autophagy dysfunction, DNA laceration, pulmonary lesion, hepatic injuries, and granuloma formation are a few. However, it must

be noted that these adverse effects were observed only when the animals were exposed directly to CNMs via various routes, such as inhalation, intravenous injection, pharyngeal aspiration, etc. as shown in Table 6. Furthermore, a 2020 report published by the OECD revealed the three most common biological side effects related to nanomaterial exposure are (i) oxidative stress, (ii) cytotoxicity, and (iii) inflammation [104]. These effects lead to tissue injuries and ultimately lung dysfunction due to the formation of mesothelioma and emphysema.

Another issue with CNMs is their biodurability/longevity and non-biodegradable nature. Pristine SWCNTs and MWCNTs do not degrade in neutral biological conditions. However, they can be degraded in an acidic medium or in the presence of peroxidases. In vitro studies have shown that SWCNTs engulfed by phagocytic cells usually generate reactive oxygen species that can break C-C and C-H bonds by activating innate peroxidases (myeloperoxidase and eosinophil peroxidase). In vivo biodurability studies of SWCNTs (diameter: 10–30 nm, length: 2–3 μm) demonstrated their presence in male CD-ICR mice 3 months after intravenous injection [105]. Likewise, MWCNTs (Diameter: 20–50 nm, length: 0.5–2 μm) stayed in the lungs of male SD rats for up to 6 months after an intratracheal instillation [106]. MWCNTs (diameter: 40–50 nm, length: 13 μm) demonstrated no mass loss by week 24 in Gamble’s solution [107]. The size of the nanotubes may also impact their biodurability. For example, SWCNTs (length: 0.5–30 μm) when incubated with HRP and H_2O_2 may result in a half-life of 80 years, while SWCNTs with a 0.1–1 μm length degraded rapidly under similar conditions [108,109].

Fullerenes also appear to be biodurable in biological and environmental conditions. Polyalkylsulfonated C-60 fullerene particles, which are highly water-soluble, were injected intraperitoneally into female SD rats at the median lethal dose (LD_{50}) of 600 mg/kg of body mass. The animals died within 30 h post-injection, and the kidneys were the main target organ [110]. In another study, fullerene particles (diameter: 60–270 nm) were engulfed by human monocytes at several sites within the cell, particularly inside the nucleus [111].

No clinical trials have been conducted so far to effectively evaluate the bedside efficacy of carbon nanomaterials-based conductive scaffolds to address ischaemic heart tissue injuries. This could largely be due to the toxic effects of CNMs as described above that might spark bioethical controversies. Therefore, CNMs-based conductive scaffolds could be useful to grow artificial heart tissues in the lab or for short-term in vivo applications, as shown in Table 5, but they do not seem worth the risk for the long term and particularly for clinical applications.

Table 6. Direct exposure of animals to carbon nanomaterials and the subsequent consequences.

| Carbon Nanomaterial | Properties | Dose | Animal | Outcomes |
|---------------------|---|-----------------------------------|---------------------|---|
| SWCNTs [112] | Diameter: 0.8–1.2 nm Length: 100–1000 nm Surface area: 508 m^2/g | 5 mg/m^3 | Female C57BL/6 mice | Four days of exposure led to inflammation with oxidative, fibrotic, and mutagenic responses. |
| SWCNTs [113] | Diameter: 2 nm Length: 0.5–40 μm Surface area: 300–600 m^2/g | 2 mg/kg | F344 rats | Presence of alveolar lesions after 21 days of exposure. |
| SWCNTs [114] | Length < 1 μm | 0.064–0.64 mg/kg | Female F344 rats | Oxidative damage to DNA in the liver and lungs. |
| MWCNTs [115] | Diameter: 10 nm Length: 200–300 nm Surface area: 253 m^2/g | 11 and 241 mg/m^3 | Male Webster rats | Fibrosis, oxidative stress, and inflammation at 241 mg/m^3 concentration while no fibrosis at 11 mg/m^3 . |

Table 6. Cont.

| Carbon Nanomaterial | Properties | Dose | Animal | Outcomes |
|------------------------------|---|--|---------------------|--|
| MWCNTs [116] | Outer diameter: 17.8 ± 6.4 nm, Length: 825 ± 174 nm Surface modification: carboxyl and hydroxyl groups Zeta potential: -48.9 ± 8 mV | Powder, <100 $\mu\text{g}/\text{rat}$ | Wister strain rats | Two years post subcutaneous implantation large agglomerates did not degrade, but smaller ones underwent lysosomal degradation. The animals did not show any sign of cancer or severe inflammation. |
| MWCNTs [117] | Diameter: 50 nm Length: 10 μm Surface area: $280 \text{ m}^2/\text{g}$ | $32.6 \text{ mg}/\text{m}^3$ | Female Kunming mice | Inhalation at the rate of 6 h/day resulted in no toxic effects after 30 days. However, severe pulmonary damage was observed after 60 days. |
| MWCNTs [118] | Diameter: 49 nm, Length: 3.86 μm | $\geq 40 \text{ }\mu\text{g}/\text{mouse}$ | Male C57BL/5 mice | Inflammation and pulmonary fibrosis with granuloma formation over 56 days of exposure. |
| C-60 fullerene [119] | Size: 0.7 nm | 0.2 mg/mouse | Male C57BL/6j mice | DNA damage in the lungs. |
| Graphene oxide [120] | Thickness: 20–30 layers | 0.12, 0.47 and 1.88 mg/L | Male SD rats | No toxic effects 28 days post-exposure |
| Reduced graphene oxide [121] | Thickness: 5 nm Zeta potential: 25 mV | 7 mg/kg | Male Wister rats | No toxic effect on hippocampus, liver, blood, and lungs 7 days post-exposure. |

11. Conclusions

The poor innate regeneration capability of the heart to heal itself is a strong driving force to find alternative therapeutic approaches to address the issue. Among many, tissue engineering has provided encouraging solutions to address the problem. In particular, carbon nanomaterials as the electroconductive component of the constructs can significantly improve the blood pumping ability of the injured heart by restoring the lost electrical functions with regenerative effects as shown in Table 5. However, long-term implantation of carbon nanomaterial-based scaffolds can pose serious complications due to their potential toxicity [122–124]. The non-biodegradable debris of nanomaterials may elicit tissue inflammation at the implantation site leading to tissue dysfunction. Therefore, new biodegradable components that can demonstrate electrical properties as high as myocardium are a dire need in cardiac tissue engineering to efficiently resolve the problem with potential clinical applications.

Author Contributions: Conceptualisation, A.U.H., F.C., F.D.M. and P.D.N.; writing—original draft preparation, A.U.H.; writing—review and editing, A.U.H., F.C., F.D.M., F.T. and P.D.N.; supervision, F.C., F.D.M. and P.D.N. All authors have read and agreed to the published version of the manuscript.

Funding: This research received no external funding.

Institutional Review Board Statement: Not applicable.

Informed Consent Statement: Not applicable.

Data Availability Statement: Not applicable.

Conflicts of Interest: The authors declare no conflict of interest.

References

1. Khan, M.A.; Hashim, M.J.; Mustafa, H.; Baniyas, M.Y.; Suwaidi, S.K.B.M.A.; AlKatheeri, R.; Alblooshi, F.M.K.; Almatrooshi, M.E.A.H.; Alzaabi, M.E.H.; Darmaki, R.S.A.; et al. Global Epidemiology of Ischemic Heart Disease: Results from the Global Burden of Disease Study. *Cureus* **2020**, *12*, e9349. [CrossRef]
2. Ambrose, J.A.; Singh, M. Pathophysiology of Coronary Artery Disease Leading to Acute Coronary Syndromes. *F1000Prime Rep.* **2015**, *7*, 8. [CrossRef] [PubMed]
3. Bergmann, O.; Zdunek, S.; Felker, A.; Salehpour, M.; Alkass, K.; Bernard, S.; Sjostrom, S.L.; Szewczykowska, M.; Jackowska, T.; dos Remedios, C.; et al. Dynamics of Cell Generation and Turnover in the Human Heart. *Cell* **2015**, *161*, 1566–1575. [CrossRef] [PubMed]
4. Sadahiro, T. Cardiac Regeneration with Pluripotent Stem Cell-Derived Cardiomyocytes and Direct Cardiac Reprogramming. *Regen. Ther.* **2019**, *11*, 95–100. [CrossRef] [PubMed]
5. Burke, A.P.; Virmani, R. Pathophysiology of Acute Myocardial Infarction. *Med. Clin. N. Am.* **2007**, *91*, 553–572. [CrossRef]
6. Heusch, G.; Gersh, B.J. The Pathophysiology of Acute Myocardial Infarction and Strategies of Protection beyond Reperfusion: A Continual Challenge. *Eur. Heart J.* **2017**, *38*, 774–784. [CrossRef] [PubMed]
7. Bangalore, S.; Fakheri, R.; Wandel, S.; Toklu, B.; Wandel, J.; Messerli, F.H. Renin Angiotensin System Inhibitors for Patients with Stable Coronary Artery Disease without Heart Failure: Systematic Review and Meta-Analysis of Randomized Trials. *BMJ* **2017**, *356*, j4. [CrossRef]
8. Freemantle, N.; Cleland, J.; Young, P.; Mason, J.; Harrison, J. β Blockade after Myocardial Infarction: Systematic Review and Meta Regression Analysis. *BMJ* **1999**, *318*, 1730–1737. [CrossRef]
9. Zhang, Q.; Xiang, J.; Wang, X.; Liu, H.; Hu, B.; Feng, M.; Fu, Q. B2-Adrenoceptor Agonist Clenbuterol Reduces Infarct Size and Myocardial Apoptosis after Myocardial Ischaemia/Reperfusion in Anaesthetized Rats. *Br. J. Pharmacol.* **2010**, *160*, 1561–1572. [CrossRef]
10. Tian, Y.; Miao, B.; Charles, E.J.; Wu, D.; Kron, I.L.; French, B.A.; Yang, Z. Stimulation of the Beta2 Adrenergic Receptor at Reperfusion Limits Myocardial Reperfusion Injury via an Interleukin-10-Dependent Anti-Inflammatory Pathway in the Spleen. *Circ. J. Off. J. Jpn. Circ. Soc.* **2018**, *82*, 2829–2836. [CrossRef]
11. Rocho-Pérez, J.A.; Garza-Treviño, E.N.; Moncada-Saucedo, N.K.; Carriquiry-Chequer, P.A.; Valencia-Gómez, L.E.; Matthews, E.R.; Gómez-Flores, V.; Simental-Mendía, M.; Delgado-Gonzalez, P.; Delgado-Gallegos, J.L.; et al. Artificial Scaffolds in Cardiac Tissue Engineering. *Life* **2022**, *12*, 1117. [CrossRef]
12. Perea-Gil, I.; Prat-Vidal, C.; Bayes-Genis, A. In Vivo Experience with Natural Scaffolds for Myocardial Infarction: The Times They Are a-Changin’. *Stem Cell Res. Ther.* **2015**, *6*, 248. [CrossRef] [PubMed]
13. Ul Haq, A.; Carotenuto, F.; De Matteis, F.; Proposito, P.; Francini, R.; Teodori, L.; Pasquo, A.; Di Nardo, P. Intrinsically Conductive Polymers for Striated Cardiac Muscle Repair. *Int. J. Mol. Sci.* **2021**, *22*, 8550. [CrossRef] [PubMed]
14. Ul Haq, A.; Carotenuto, F.; Di Nardo, P.; Francini, R.; Proposito, P.; Pescosolido, F.; De Matteis, F. Extrinsically Conductive Nanomaterials for Cardiac Tissue Engineering Applications. *Micromachines* **2021**, *12*, 914. [CrossRef]
15. Ryoo, S.M.; Kim, W.Y. Clinical Applications of Lactate Testing in Patients with Sepsis and Septic Shock. *J. Emerg. Crit. Care Med.* **2018**, *2*, 14. [CrossRef]
16. Braasch, W.; Gudbjarnason, S.; Puri, P.S.; Ravens, K.G.; Bing, R.J. Early Changes in Energy Metabolism in the Myocardium Following Acute Coronary Artery Occlusion in Anesthetized Dogs. *Circ. Res.* **1968**, *23*, 429–438. [CrossRef] [PubMed]
17. Frangogiannis, N.G. Pathophysiology of Myocardial Infarction. In *Comprehensive Physiology*; American Physiological Society: Bethesda, MD, USA, 2015; pp. 1841–1875. [CrossRef]
18. Carmeliet, E. Cardiac Ionic Currents and Acute Ischemia: From Channels to Arrhythmias. *Physiol. Rev.* **1999**, *79*, 917–1017. [CrossRef] [PubMed]
19. Kléber, A.G. Resting Membrane Potential, Extracellular Potassium Activity, and Intracellular Sodium Activity during Acute Global Ischemia in Isolated Perfused Guinea Pig Hearts. *Circ. Res.* **1983**, *52*, 442–450. [CrossRef]
20. Coraboeuf, E. Acidosis-Induced Abnormal Repolarization and Repetitive Activity in Isolated Dog Purkinje Fibers. *ACIDOSIS-Induc. Abnorm. REPOLARIZATION REPETITIVE Act. Isol. DOG PURKINJE FIBERS*. 1980. Available online: <https://pascal-francis.inist.fr/vibad/index.php?action=getRecordDetail&idt=PASCAL8050486952> (accessed on 25 November 2022).
21. van den Borne, S.W.M.; Diez, J.; Blankesteijn, W.M.; Verjans, J.; Hofstra, L.; Narula, J. Myocardial Remodeling after Infarction: The Role of Myofibroblasts. *Nat. Rev. Cardiol.* **2010**, *7*, 30–37. [CrossRef]
22. Thygesen, K.; Alpert, J.S.; Jaffe, A.S.; Simoons, M.L.; Chaitman, B.R.; White, H.D.; Writing Group on the Joint ESC/ACCF/AHA/WHF Task Force for the Universal Definition of Myocardial Infarction; Katus, H.A.; Apple, F.S.; Lindahl, B. Third Universal Definition of Myocardial Infarction. *Eur. Heart J.* **2012**, *33*, 2551–2567. [CrossRef]
23. Gourdie, R.G.; Severs, N.J.; Green, C.R.; Rothery, S.; Germroth, P.; Thompson, R.P. The Spatial Distribution and Relative Abundance of Gap-Junctional Connexin40 and Connexin43 Correlate to Functional Properties of Components of the Cardiac Atrioventricular Conduction System. *J. Cell Sci.* **1993**, *105*, 985–991. [CrossRef] [PubMed]
24. Beardslee, M.A.; Lerner, D.L.; Tadros, P.N.; Laing, J.G.; Beyers, E.C.; Yamada, K.A.; Kléber, A.G.; Schuessler, R.B.; Saffitz, J.E. Dephosphorylation and Intracellular Redistribution of Ventricular Connexin43 during Electrical Uncoupling Induced by Ischemia. *Circ. Res.* **2000**, *87*, 656–662. [CrossRef] [PubMed]

25. Lerner, D.L.; Yamada, K.A.; Schuessler, R.B.; Saffitz, J.E. Accelerated Onset and Increased Incidence of Ventricular Arrhythmias Induced by Ischemia in Cx43-Deficient Mice. *Circulation* **2000**, *101*, 547–552. [[CrossRef](#)] [[PubMed](#)]
26. Cao, N.; Huang, Y.; Zheng, J.; Spencer, C.I.; Zhang, Y.; Fu, J.-D.; Nie, B.; Xie, M.; Zhang, M.; Wang, H.; et al. Conversion of Human Fibroblasts into Functional Cardiomyocytes by Small Molecules. *Science* **2016**, *352*, 1216–1220. [[CrossRef](#)]
27. Roell, W.; Lewalter, T.; Sasse, P.; Tallini, Y.N.; Choi, B.-R.; Breitbach, M.; Doran, R.; Becher, U.M.; Hwang, S.-M.; Bostani, T.; et al. Engraftment of Connexin 43-Expressing Cells Prevents Post-Infarct Arrhythmia. *Nature* **2007**, *450*, 819–824. [[CrossRef](#)]
28. Fomovsky, G.M.; Clark, S.A.; Parker, K.M.; Ailawadi, G.; Holmes, J.W. Anisotropic Reinforcement of Acute Anteroapical Infarcts Improves Pump Function. *Circ. Heart Fail.* **2012**, *5*, 515–522. [[CrossRef](#)]
29. Ursell, P.C.; Gardner, P.I.; Albala, A.; Fenoglio, J.J.; Wit, A.L. Structural and Electrophysiological Changes in the Epicardial Border Zone of Canine Myocardial Infarcts during Infarct Healing. *Circ. Res.* **1985**, *56*, 436–451. [[CrossRef](#)]
30. Driesen, R.B.; Verheyen, F.K.; Dijkstra, P.; Thoné, F.; Cleutjens, J.P.; Lenders, M.-H.; Ramaekers, F.C.S.; Borgers, M. Structural Remodelling of Cardiomyocytes in the Border Zone of Infarcted Rabbit Heart. *Mol. Cell. Biochem.* **2007**, *302*, 225–232. [[CrossRef](#)]
31. Jugdutt, B.I. Ventricular Remodeling After Infarction and the Extracellular Collagen Matrix. *Circulation* **2003**, *108*, 1395–1403. [[CrossRef](#)]
32. Baba, S.; Dun, W.; Cabo, C.; Boyden, P.A. Remodeling in Cells From Different Regions of the Reentrant Circuit During Ventricular Tachycardia. *Circulation* **2005**, *112*, 2386–2396. [[CrossRef](#)]
33. Dun, W.; Lowe, J.S.; Wright, P.; Hund, T.J.; Mohler, P.J.; Boyden, P.A. Ankyrin-G Participates in INa Remodeling in Myocytes from the Border Zones of Infarcted Canine Heart. *PLoS ONE* **2013**, *8*, e78087. [[CrossRef](#)] [[PubMed](#)]
34. Lue, W.M.; Boyden, P.A. Abnormal Electrical Properties of Myocytes from Chronically Infarcted Canine Heart. Alterations in Vmax and the Transient Outward Current. *Circulation* **1992**, *85*, 1175–1188. [[CrossRef](#)] [[PubMed](#)]
35. Pinto, J.M.B.; Boyden, P.A. Electrical Remodeling in Ischemia and Infarction. *Cardiovasc. Res.* **1999**, *42*, 284–297. [[CrossRef](#)] [[PubMed](#)]
36. Ongstad, E.L.; Gourdie, R.G. Can Heart Function Lost to Disease Be Regenerated by Therapeutic Targeting of Cardiac Scar Tissue? *Semin. Cell Dev. Biol.* **2016**, *58*, 41–54. [[CrossRef](#)] [[PubMed](#)]
37. Bers, D.M. Calcium Cycling and Signaling in Cardiac Myocytes. *Annu. Rev. Physiol.* **2008**, *70*, 23–49. [[CrossRef](#)]
38. Rosenbaum, D.S.; Jackson, L.E.; Smith, J.M.; Garan, H.; Ruskin, J.N.; Cohen, R.J. Electrical Alternans and Vulnerability to Ventricular Arrhythmias. *N. Engl. J. Med.* **1994**, *330*, 235–241. [[CrossRef](#)]
39. Iijima, K.; Geshi, E.; Nomizo, A.; Arata, Y.; Katagiri, T. Alterations in Sarcoplasmic Reticulum and Angiotensin II Type 1 Receptor Gene Expression after Myocardial Infarction in Rats. *Jpn. Circ. J.* **1998**, *62*, 449–454. [[CrossRef](#)]
40. Frangogiannis, N.G.; Smith, C.W.; Entman, M.L. The Inflammatory Response in Myocardial Infarction. *Cardiovasc. Res.* **2002**, *53*, 31–47. [[CrossRef](#)]
41. Rienks, M.; Papageorgiou, A.-P.; Frangogiannis, N.G.; Heymans, S. Myocardial Extracellular Matrix: An Ever-Changing and Diverse Entity. *Circ. Res.* **2014**, *114*, 872–888. [[CrossRef](#)]
42. Khodayari, S.; Khodayari, H.; Amiri, A.Z.; Eslami, M.; Farhud, D.; Hescheler, J.; Nayernia, K. Inflammatory Microenvironment of Acute Myocardial Infarction Prevents Regeneration of Heart with Stem Cells Therapy. *Cell. Physiol. Biochem. Int. J. Exp. Cell. Physiol. Biochem. Pharmacol.* **2019**, *53*, 887–909. [[CrossRef](#)]
43. Ma, Y.; de Castro Brás, L.E.; Toba, H.; Iyer, R.P.; Hall, M.E.; Winniford, M.D.; Lange, R.A.; Tyagi, S.C.; Lindsey, M.L. Myofibroblasts and the Extracellular Matrix Network in Post-Myocardial Infarction Cardiac Remodeling. *Pflugers Arch.* **2014**, *466*, 1113–1127. [[CrossRef](#)] [[PubMed](#)]
44. Xing, Y.; Lv, A.; Wang, L.; Yan, X.; Zhao, W.; Cao, F. Engineered Myocardial Tissues Constructed in Vivo Using Cardiomyocyte-like Cells Derived from Bone Marrow Mesenchymal Stem Cells in Rats. *J. Biomed. Sci.* **2012**, *19*, 6. [[CrossRef](#)]
45. Morritt, A.N.; Bortolotto, S.K.; Dilley, R.J.; Han, X.; Kompa, A.R.; McCombe, D.; Wright, C.E.; Itescu, S.; Angus, J.A.; Morrison, W.A. Cardiac Tissue Engineering in an In Vivo Vascularized Chamber. *Circulation* **2007**, *115*, 353–360. [[CrossRef](#)] [[PubMed](#)]
46. Gao, L.; Kupfer, M.E.; Jung, J.P.; Yang, L.; Zhang, P.; Da Sie, Y.; Tran, Q.; Ajeti, V.; Freeman, B.T.; Fast, V.G.; et al. Myocardial Tissue Engineering With Cells Derived From Human-Induced Pluripotent Stem Cells and a Native-Like, High-Resolution, 3-Dimensionally Printed Scaffold. *Circ. Res.* **2017**, *120*, 1318–1325. [[CrossRef](#)]
47. Madden, L.R.; Mortisen, D.J.; Sussman, E.M.; Dupras, S.K.; Fugate, J.A.; Cuy, J.L.; Hauch, K.D.; Laflamme, M.A.; Murry, C.E.; Ratner, B.D. Proangiogenic Scaffolds as Functional Templates for Cardiac Tissue Engineering. *Proc. Natl. Acad. Sci. USA* **2010**, *107*, 15211–15216. [[CrossRef](#)] [[PubMed](#)]
48. Wendel, J.S.; Ye, L.; Zhang, P.; Tranquillo, R.T.; Zhang, J.J. Functional Consequences of a Tissue-Engineered Myocardial Patch for Cardiac Repair in a Rat Infarct Model. *Tissue Eng. Part A* **2014**, *20*, 1325–1335. [[CrossRef](#)] [[PubMed](#)]
49. Stoppel, W.L.; Hu, D.; Domian, I.J.; Kaplan, D.L.; Black, L.D. Anisotropic Silk Biomaterials Containing Cardiac Extracellular Matrix for Cardiac Tissue Engineering. *Biomed. Mater.* **2015**, *10*, 034105. [[CrossRef](#)] [[PubMed](#)]
50. Stuckey, D.J.; Ishii, H.; Chen, Q.-Z.; Boccaccini, A.R.; Hansen, U.; Carr, C.A.; Roether, J.A.; Jawad, H.; Tyler, D.J.; Ali, N.N.; et al. Magnetic Resonance Imaging Evaluation of Remodeling by Cardiac Elastomeric Tissue Scaffold Biomaterials in a Rat Model of Myocardial Infarction. *Tissue Eng. Part A* **2010**, *16*, 3395–3402. [[CrossRef](#)]
51. Ban, K.; Park, H.-J.; Kim, S.; Andukuri, A.; Cho, K.-W.; Hwang, J.W.; Cha, H.J.; Kim, S.Y.; Kim, W.-S.; Jun, H.-W.; et al. Cell Therapy with Embryonic Stem Cell-Derived Cardiomyocytes Encapsulated in Injectable Nanomatrix Gel Enhances Cell Engraftment and Promotes Cardiac Repair. *ACS Nano* **2014**, *8*, 10815–10825. [[CrossRef](#)]

52. Sun, H.; Lü, S.; Jiang, X.-X.; Li, X.; Li, H.; Lin, Q.; Mou, Y.; Zhao, Y.; Han, Y.; Zhou, J.; et al. Carbon Nanotubes Enhance Intercalated Disc Assembly in Cardiac Myocytes via the B1-Integrin-Mediated Signaling Pathway. *Biomaterials* **2015**, *55*, 84–95. [[CrossRef](#)]
53. Ahmadi, P.; Nazeri, N.; Derakhshan, M.A.; Ghanbari, H. Preparation and Characterization of Polyurethane/Chitosan/CNT Nanofibrous Scaffold for Cardiac Tissue Engineering. *Int. J. Biol. Macromol.* **2021**, *180*, 590–598. [[CrossRef](#)] [[PubMed](#)]
54. Ma, J.; Wang, J.-N.; Tsai, C.-J.; Nussinov, R.; Ma, B. Diameters of Single-Walled Carbon Nanotubes (SWCNTs) and Related Nanochemistry and Nanobiology. *Front. Mater. Sci. China* **2010**, *4*, 17–28. [[CrossRef](#)]
55. Sakurai, S.; Inaguma, M.; Futaba, D.N.; Yumura, M.; Hata, K. A Fundamental Limitation of Small Diameter Single-Walled Carbon Nanotube Synthesis-A Scaling Rule of the Carbon Nanotube Yield with Catalyst Volume. *Materials* **2013**, *6*, 2633–2641. [[CrossRef](#)] [[PubMed](#)]
56. Lanone, S.; Andujar, P.; Kermanizadeh, A.; Boczkowski, J. Determinants of Carbon Nanotube Toxicity. *Adv. Drug Deliv. Rev.* **2013**, *65*, 2063–2069. [[CrossRef](#)] [[PubMed](#)]
57. Saito, N.; Haniu, H.; Usui, Y.; Aoki, K.; Hara, K.; Takanashi, S.; Shimizu, M.; Narita, N.; Okamoto, M.; Kobayashi, S.; et al. Safe Clinical Use of Carbon Nanotubes as Innovative Biomaterials. *Chem. Rev.* **2014**, *114*, 6040–6079. [[CrossRef](#)] [[PubMed](#)]
58. Roshanbinfar, K.; Hilborn, J.; Varghese, P.O.; Oommen, P.O. Injectable and Thermoresponsive Pericardial Matrix Derived Conductive Scaffold for Cardiac Tissue Engineering. *RSC Adv.* **2017**, *7*, 31980–31988. [[CrossRef](#)]
59. Ramón-Azcón, J.; Ahadian, S.; Estili, M.; Liang, X.; Ostrovidov, S.; Kaji, H.; Shiku, H.; Ramalingam, M.; Nakajima, K.; Sakka, Y.; et al. Dielectrophoretically Aligned Carbon Nanotubes to Control Electrical and Mechanical Properties of Hydrogels to Fabricate Contractile Muscle Myofibers. *Adv. Mater.* **2013**, *25*, 4028–4034. [[CrossRef](#)]
60. Abedi, A.; Bakhshandeh, B.; Babaie, A.; Mohammadnejad, J.; Vahdat, S.; Mombeiny, R.; Moosavi, S.R.; Amini, J.; Tayebi, L. Concurrent Application of Conductive Biopolymeric Chitosan/ Polyvinyl Alcohol/ MWCNTs Nanofibers, Intracellular Signaling Manipulating Molecules and Electrical Stimulation for More Effective Cardiac Tissue Engineering. *Mater. Chem. Phys.* **2021**, *258*, 123842. [[CrossRef](#)]
61. Ahadian, S.; Yamada, S.; Ramón-Azcón, J.; Estili, M.; Liang, X.; Nakajima, K.; Shiku, H.; Khademhosseini, A.; Matsue, T. Hybrid Hydrogel-Aligned Carbon Nanotube Scaffolds to Enhance Cardiac Differentiation of Embryoid Bodies. *Acta Biomater.* **2016**, *31*, 134–143. [[CrossRef](#)]
62. Ahadian, S.; Yamada, S.; Estili, M.; Liang, X.; Banan Sadeghian, R.; Nakajima, K.; Shiku, H.; Matsue, T.; Khademhosseini, A. Carbon Nanotubes Embedded in Embryoid Bodies Direct Cardiac Differentiation. *Biomed. Microdevices* **2017**, *19*, 57. [[CrossRef](#)]
63. Mehrotra, S.; Singh, R.D.; Bandyopadhyay, A.; Janani, G.; Dey, S.; Mandal, B.B. Engineering Microsphere-Loaded Non-Mulberry Silk-Based 3D Bioprinted Vascularized Cardiac Patches with Oxygen-Releasing and Immunomodulatory Potential. *ACS Appl. Mater. Interfaces* **2021**, *13*, 50744–50759. [[CrossRef](#)] [[PubMed](#)]
64. Shin, S.R.; Jung, S.M.; Zalabany, M.; Kim, K.; Zorlutuna, P.; Kim, S.B.; Nikkhah, M.; Khabiry, M.; Azize, M.; Kong, J.; et al. Carbon-Nanotube-Embedded Hydrogel Sheets for Engineering Cardiac Constructs and Bioactuators. *ACS Nano* **2013**, *7*, 2369–2380. [[CrossRef](#)] [[PubMed](#)]
65. Sun, H.; Zhou, J.; Huang, Z.; Qu, L.; Lin, N.; Liang, C.; Dai, R.; Tang, L.; Tian, F. Carbon Nanotube-Incorporated Collagen Hydrogels Improve Cell Alignment and the Performance of Cardiac Constructs. *Int. J. Nanomed.* **2017**, *12*, 3109–3120. [[CrossRef](#)] [[PubMed](#)]
66. Mehdikhani, M.; Ghaziof, S. Electrically Conductive Poly-ε-Caprolactone/Polyethylene Glycol/Multi-Wall Carbon Nanotube Nanocomposite Scaffolds Coated with Fibrin Glue for Myocardial Tissue Engineering. *Appl. Phys. A* **2018**, *124*, 77. [[CrossRef](#)]
67. Ren, J.; Xu, Q.; Chen, X.; Li, W.; Guo, K.; Zhao, Y.; Wang, Q.; Zhang, Z.; Peng, H.; Li, Y.-G. Superaligned Carbon Nanotubes Guide Oriented Cell Growth and Promote Electrophysiological Homogeneity for Synthetic Cardiac Tissues. *Adv. Mater.* **2017**, *29*, 1702713. [[CrossRef](#)]
68. Martinelli, V.; Cellot, G.; Toma, F.M.; Long, C.S.; Caldwell, J.H.; Zentilin, L.; Giacca, M.; Turco, A.; Prato, M.; Ballerini, L.; et al. Carbon Nanotubes Promote Growth and Spontaneous Electrical Activity in Cultured Cardiac Myocytes. *Nano Lett.* **2012**, *12*, 1831–1838. [[CrossRef](#)]
69. Kharaziha, M.; Shin, S.R.; Nikkhah, M.; Topkaya, S.N.; Masoumi, N.; Annabi, N.; Dokmeci, M.R.; Khademhosseini, A. Tough and Flexible CNT-Polymeric Hybrid Scaffolds for Engineering Cardiac Constructs. *Biomaterials* **2014**, *35*, 7346–7354. [[CrossRef](#)]
70. Wang, Y.; Dong, Y.; Chen, P.; Chen, R.; Li, Y.; Du, W.; Liu, B.-F. Reduced Graphene Oxide Foam Templated by Nickel Foam for Organ-on-a-Chip Engineering of Cardiac Constructs. *Mater. Sci. Eng. C Mater. Biol. Appl.* **2020**, *117*, 111344. [[CrossRef](#)]
71. Karimi Hajishoreh, N.; Baheiraei, N.; Naderi, N.; Salehnia, M. Reduced Graphene Oxide Facilitates Biocompatibility of Alginate for Cardiac Repair. *J. Bioact. Compat. Polym.* **2020**, *35*, 363–377. [[CrossRef](#)]
72. Norahan, M.H.; Pourmokhtari, M.; Saeb, M.R.; Bakhshi, B.; Soufi Zomorrod, M.; Baheiraei, N. Electroactive Cardiac Patch Containing Reduced Graphene Oxide with Potential Antibacterial Properties. *Mater. Sci. Eng. C Mater. Biol. Appl.* **2019**, *104*, 109921. [[CrossRef](#)]
73. Zhou, J.; Yang, X.; Liu, W.; Wang, C.; Shen, Y.; Zhang, F.; Zhu, H.; Sun, H.; Chen, J.; Lam, J.; et al. Injectable OPF/Graphene Oxide Hydrogels Provide Mechanical Support and Enhance Cell Electrical Signaling after Implantation into Myocardial Infarct. *Theranostics* **2018**, *8*, 3317–3330. [[CrossRef](#)] [[PubMed](#)]
74. Talebi, A.; Labbaf, S.; Karimzadeh, F.; Masaali, E.; Nasr Esfahani, M.-H. Electroconductive Graphene-Containing Polymeric Patch: A Promising Platform for Future Cardiac Repair. *ACS Biomater. Sci. Eng.* **2020**, *6*, 4214–4224. [[CrossRef](#)] [[PubMed](#)]

75. Shin, S.R.; Zihlmann, C.; Akbari, M.; Assawes, P.; Cheung, L.; Zhang, K.; Manoharan, V.; Zhang, Y.S.; Yükksekaya, M.; Wan, K.-T.; et al. Reduced Graphene Oxide-GelMA Hybrid Hydrogels as Scaffolds for Cardiac Tissue Engineering. *Small Weinh. Bergstr. Ger.* **2016**, *12*, 3677–3689. [[CrossRef](#)] [[PubMed](#)]
76. Tsui, J.H.; Leonard, A.; Camp, N.D.; Long, J.T.; Nawas, Z.Y.; Chavanachat, R.; Smith, A.S.T.; Choi, J.S.; Dong, Z.; Ahn, E.H.; et al. Tunable Electroconductive Decellularized Extracellular Matrix Hydrogels for Engineering Human Cardiac Microphysiological Systems. *Biomaterials* **2021**, *272*, 120764. [[CrossRef](#)]
77. Hitscherich, P.; Aphale, A.; Gordan, R.; Whitaker, R.; Singh, P.; Xie, L.-H.; Patra, P.; Lee, E.J. Electroactive Graphene Composite Scaffolds for Cardiac Tissue Engineering. *J. Biomed. Mater. Res. A* **2018**, *106*, 2923–2933. [[CrossRef](#)]
78. Saravanan, S.; Sareen, N.; Abu-El-Rub, E.; Ashour, H.; Sequiera, G.L.; Ammar, H.I.; Gopinath, V.; Shamaa, A.A.; Sayed, S.S.E.; Moudgil, M.; et al. Graphene Oxide-Gold Nanosheets Containing Chitosan Scaffold Improves Ventricular Contractility and Function After Implantation into Infarcted Heart. *Sci. Rep.* **2018**, *8*, 15069. [[CrossRef](#)]
79. Li, X.-P.; Qu, K.-Y.; Zhou, B.; Zhang, F.; Wang, Y.-Y.; Abodunrin, O.D.; Zhu, Z.; Huang, N.-P. Electrical Stimulation of Neonatal Rat Cardiomyocytes Using Conductive Polydopamine-Reduced Graphene Oxide-Hybrid Hydrogels for Constructing Cardiac Microtissues. *Colloids Surf. B Biointerfaces* **2021**, *205*, 111844. [[CrossRef](#)]
80. Zhao, G.; Feng, Y.; Xue, L.; Cui, M.; Zhang, Q.; Xu, F.; Peng, N.; Jiang, Z.; Gao, D.; Zhang, X. Anisotropic Conductive Reduced Graphene Oxide/Silk Matrices Promote Post-Infarction Myocardial Function by Restoring Electrical Integrity. *Acta Biomater.* **2022**, *139*, 190–203. [[CrossRef](#)]
81. Goodarzi, S.; Da Ros, T.; Conde, J.; Sefat, F.; Mozafari, M. Fullerene: Biomedical Engineers Get to Revisit an Old Friend. *Mater. Today* **2017**, *20*, 460–480. [[CrossRef](#)]
82. Hao, T.; Zhou, J.; Lü, S.; Yang, B.; Wang, Y.; Fang, W.; Jiang, X.; Lin, Q.; Li, J.; Wang, C. Fullerene Mediates Proliferation and Cardiomyogenic Differentiation of Adipose-Derived Stem Cells via Modulation of MAPK Pathway and Cardiac Protein Expression. *Int. J. Nanomed.* **2016**, *11*, 269–283. [[CrossRef](#)]
83. Hao, T.; Li, J.; Yao, F.; Dong, D.; Wang, Y.; Yang, B.; Wang, C. Injectable Fullerenol/Alginate Hydrogel for Suppression of Oxidative Stress Damage in Brown Adipose-Derived Stem Cells and Cardiac Repair. *ACS Nano* **2017**, *11*, 5474–5488. [[CrossRef](#)] [[PubMed](#)]
84. Minami, K.; Kasuya, Y.; Yamazaki, T.; Ji, Q.; Nakanishi, W.; Hill, J.P.; Sakai, H.; Ariga, K. Highly Ordered 1D Fullerene Crystals for Concurrent Control of Macroscopic Cellular Orientation and Differentiation toward Large-Scale Tissue Engineering. *Adv. Mater.* **2015**, *27*, 4020–4026. [[CrossRef](#)] [[PubMed](#)]
85. Tashakori-Miyanroudi, M.; Rakhshan, K.; Ramez, M.; Asgarian, S.; Janzadeh, A.; Azizi, Y.; Seifalian, A.; Ramezani, F. Conductive Carbon Nanofibers Incorporated into Collagen Bio-Scaffold Assists Myocardial Injury Repair. *Int. J. Biol. Macromol.* **2020**, *163*, 1136–1146. [[CrossRef](#)] [[PubMed](#)]
86. Mehrabi, A.; Baheiraei, N.; Adabi, M.; Amirkhani, Z. Development of a Novel Electroactive Cardiac Patch Based on Carbon Nanofibers and Gelatin Encouraging Vascularization. *Appl. Biochem. Biotechnol.* **2020**, *190*, 931–948. [[CrossRef](#)] [[PubMed](#)]
87. Martins, A.M.; Eng, G.; Caridade, S.G.; Mano, J.F.; Reis, R.L.; Vunjak-Novakovic, G. Electrically Conductive Chitosan/Carbon Scaffolds for Cardiac Tissue Engineering. *Biomacromolecules* **2014**, *15*, 635–643. [[CrossRef](#)] [[PubMed](#)]
88. Fu, S.; Ping, P.; Wang, F.; Luo, L. Synthesis, Function, Metabolism and Application of Natriuretic Peptides in Heart Failure. *J. Biol. Eng.* **2018**, *12*, 2. [[CrossRef](#)]
89. Meng, J.; Xiao, B.; Wu, F.; Sun, L.; Li, B.; Guo, W.; Hu, X.; Xu, X.; Wen, T.; Liu, J.; et al. Co-Axial Fibrous Scaffolds Integrating with Carbon Fiber Promote Cardiac Tissue Regeneration Post Myocardial Infarction. *Mater. Today Bio* **2022**, *16*, 100415. [[CrossRef](#)]
90. Asiri, A.M.; Marwani, H.M.; Khan, S.B.; Webster, T.J. Greater Cardiomyocyte Density on Aligned Compared with Random Carbon Nanofibers in Polymer Composites. *Int. J. Nanomed.* **2014**, *9*, 5533–5539. [[CrossRef](#)]
91. Stoppel, W.L.; Kaplan, D.L.; Black, L.D. Electrical and Mechanical Stimulation of Cardiac Cells and Tissue Constructs. *Adv. Drug Deliv. Rev.* **2016**, *96*, 135–155. [[CrossRef](#)]
92. Passier, R.; Zeng, H.; Frey, N.; Naya, F.J.; Nicol, R.L.; McKinsey, T.A.; Overbeek, P.; Richardson, J.A.; Grant, S.R.; Olson, E.N. CaM Kinase Signaling Induces Cardiac Hypertrophy and Activates the MEF2 Transcription Factor in Vivo. *J. Clin. Investig.* **2000**, *105*, 1395–1406. [[CrossRef](#)]
93. Adachi, A.; Takahashi, T.; Ogata, T.; Imoto-Tsubakimoto, H.; Nakanishi, N.; Ueyama, T.; Matsubara, H. NFAT5 Regulates the Canonical Wnt Pathway and Is Required for Cardiomyogenic Differentiation. *Biochem. Biophys. Res. Commun.* **2012**, *426*, 317–323. [[CrossRef](#)] [[PubMed](#)]
94. Chen, Y.; Cao, X. NFAT Directly Regulates Nkx2-5 Transcription during Cardiac Cell Differentiation. *Biol. Cell* **2009**, *101*, 335–349. [[CrossRef](#)] [[PubMed](#)]
95. Xia, Y.; McMillin, J.B.; Lewis, A.; Moore, M.; Zhu, W.G.; Williams, R.S.; Kellems, R.E. Electrical Stimulation of Neonatal Cardiac Myocytes Activates the NFAT3 and GATA4 Pathways and Up-Regulates the Adenylosuccinate Synthetase 1 Gene. *J. Biol. Chem.* **2000**, *275*, 1855–1863. [[CrossRef](#)]
96. Watt, A.J.; Battle, M.A.; Li, J.; Duncan, S.A. GATA4 Is Essential for Formation of the Proepicardium and Regulates Cardiogenesis. *Proc. Natl. Acad. Sci. USA* **2004**, *101*, 12573–12578. [[CrossRef](#)] [[PubMed](#)]
97. Saadane, N.; Alpert, L.; Chalifour, L.E. Expression of Immediate Early Genes, GATA-4, and Nkx-2.5 in Adrenergic-Induced Cardiac Hypertrophy and during Regression in Adult Mice. *Br. J. Pharmacol.* **1999**, *127*, 1165–1176. [[CrossRef](#)] [[PubMed](#)]
98. Wei, B.; Jin, J.-P. TNNT1, TNNT2, and TNNT3: Isoform Genes, Regulation, and Structure–Function Relationships. *Gene* **2016**, *582*, 1–13. [[CrossRef](#)]

99. Kotini, M.; Barriga, E.H.; Leslie, J.; Gentzel, M.; Rauschenberger, V.; Schambony, A.; Mayor, R. Gap Junction Protein Connexin-43 Is a Direct Transcriptional Regulator of N-Cadherin in Vivo. *Nat. Commun.* **2018**, *9*, 3846. [CrossRef]
100. Zhou, J.; Chen, J.; Sun, H.; Qiu, X.; Mou, Y.; Liu, Z.; Zhao, Y.; Li, X.; Han, Y.; Duan, C.; et al. Engineering the Heart: Evaluation of Conductive Nanomaterials for Improving Implant Integration and Cardiac Function. *Sci. Rep.* **2014**, *4*, 3733. [CrossRef]
101. Li, X.; Zhou, J.; Liu, Z.; Chen, J.; Lü, S.; Sun, H.; Li, J.; Lin, Q.; Yang, B.; Duan, C.; et al. A PNIPAAm-Based Thermosensitive Hydrogel Containing SWCNTs for Stem Cell Transplantation in Myocardial Repair. *Biomaterials* **2014**, *35*, 5679–5688. [CrossRef]
102. Bao, R.; Tan, B.; Liang, S.; Zhang, N.; Wang, W.; Liu, W. A π - π Conjugation-Containing Soft and Conductive Injectable Polymer Hydrogel Highly Efficiently Rebuilds Cardiac Function after Myocardial Infarction. *Biomaterials* **2017**, *122*, 63–71. [CrossRef]
103. Yuan, Z.; Qin, Q.; Yuan, M.; Wang, H.; Li, R. Development and Novel Design of Clustery Graphene Oxide Formed Conductive Silk Hydrogel Cell Vesicle to Repair and Routine Care of Myocardial Infarction: Investigation of Its Biological Activity for Cell Delivery Applications. *J. Drug Deliv. Sci. Technol.* **2020**, *60*, 102001. [CrossRef]
104. Advancing Adverse Outcome Pathway (AOP) Development for Nanomaterial Risk Assessment and Categorisation Part 2: Case Study on Tissue Injury; Safety of Manufactured Nanomaterials. Available online: <https://www.oecd.org/officialdocuments/publicdisplaydocumentpdf/?cote=env/jm/%20mono> (accessed on 25 November 2022).
105. Yang, S.-T.; Wang, X.; Jia, G.; Gu, Y.; Wang, T.; Nie, H.; Ge, C.; Wang, H.; Liu, Y. Long-Term Accumulation and Low Toxicity of Single-Walled Carbon Nanotubes in Intravenously Exposed Mice. *Toxicol. Lett.* **2008**, *181*, 182–189. [CrossRef] [PubMed]
106. Elgrabli, D.; Floriani, M.; Abella-Gallart, S.; Meunier, L.; Gamez, C.; Delalain, P.; Rogerieux, F.; Boczkowski, J.; Lacroix, G. Biodistribution and Clearance of Instilled Carbon Nanotubes in Rat Lung. *Part. Fibre Toxicol.* **2008**, *5*, 20. [CrossRef] [PubMed]
107. Osmond-McLeod, M.J.; Poland, C.A.; Murphy, F.; Waddington, L.; Morris, H.; Hawkins, S.C.; Clark, S.; Aitken, R.; McCall, M.J.; Donaldson, K. Durability and Inflammogenic Impact of Carbon Nanotubes Compared with Asbestos Fibres. *Part. Fibre Toxicol.* **2011**, *8*, 15. [CrossRef] [PubMed]
108. Flores-Cervantes, D.X.; Maes, H.M.; Schäffer, A.; Hollender, J.; Kohler, H.-P.E. Slow Biotransformation of Carbon Nanotubes by Horseradish Peroxidase. *Environ. Sci. Technol.* **2014**, *48*, 4826–4834. [CrossRef]
109. Russier, J.; Ménard-Moyon, C.; Venturelli, E.; Gravel, E.; Marcolongo, G.; Meneghetti, M.; Doris, E.; Bianco, A. Oxidative Biodegradation of Single- and Multi-Walled Carbon Nanotubes. *Nanoscale* **2011**, *3*, 893–896. [CrossRef]
110. Chen, H.H.; Yu, C.; Ueng, T.H.; Chen, S.; Chen, B.J.; Huang, K.J.; Chiang, L.Y. Acute and Subacute Toxicity Study of Water-Soluble Polyalkylsulfonated C60 in Rats. *Toxicol. Pathol.* **1998**, *26*, 143–151. [CrossRef]
111. Porter, A.E.; Muller, K.; Skepper, J.; Midgley, P.; Welland, M. Uptake of C60 by Human Monocyte Macrophages, Its Localization and Implications for Toxicity: Studied by High Resolution Electron Microscopy and Electron Tomography. *Acta Biomater.* **2006**, *2*, 409–419. [CrossRef]
112. Shvedova, A.A.; Kisin, E.; Murray, A.R.; Johnson, V.J.; Gorelik, O.; Arepalli, S.; Hubbs, A.F.; Mercer, R.R.; Keohavong, P.; Sussman, N.; et al. Inhalation vs. Aspiration of Single-Walled Carbon Nanotubes in C57BL/6 Mice: Inflammation, Fibrosis, Oxidative Stress, and Mutagenesis. *Am. J. Physiol. Lung Cell. Mol. Physiol.* **2008**, *295*, L552–L565. [CrossRef]
113. Mangum, J.B.; Turpin, E.A.; Antao-Menezes, A.; Cesta, M.F.; Bermudez, E.; Bonner, J.C. Single-Walled Carbon Nanotube (SWCNT)-Induced Interstitial Fibrosis in the Lungs of Rats Is Associated with Increased Levels of PDGF MRNA and the Formation of Unique Interstitial Carbon Structures That Bridge Alveolar Macrophages in Situ. *Part. Fibre Toxicol.* **2006**, *3*, 15. [CrossRef]
114. Folkmann, J.K.; Risom, L.; Jacobsen, N.R.; Wallin, H.; Loft, S.; Møller, P. Oxidatively Damaged DNA in Rats Exposed by Oral Gavage to C60 Fullerenes and Single-Walled Carbon Nanotubes. *Environ. Health Perspect.* **2009**, *117*, 703–708. [CrossRef] [PubMed]
115. Ellinger-Ziegelbauer, H.; Pauluhn, J. Pulmonary Toxicity of Multi-Walled Carbon Nanotubes (Baytubes) Relative to Alpha-Quartz Following a Single 6h Inhalation Exposure of Rats and a 3 Months Post-Exposure Period. *Toxicology* **2009**, *266*, 16–29. [CrossRef] [PubMed]
116. Sato, Y.; Yokoyama, A.; Nodasaka, Y.; Kohgo, T.; Motomiya, K.; Matsumoto, H.; Nakazawa, E.; Numata, T.; Zhang, M.; Yudasaka, M.; et al. Long-Term Biopersistence of Tangled Oxidized Carbon Nanotubes inside and Outside Macrophages in Rat Subcutaneous Tissue. *Sci. Rep.* **2013**, *3*, 2516. [CrossRef]
117. Li, J.-G.; Li, W.-X.; Xu, J.-Y.; Cai, X.-Q.; Liu, R.-L.; Li, Y.-J.; Zhao, Q.-F.; Li, Q.-N. Comparative Study of Pathological Lesions Induced by Multiwalled Carbon Nanotubes in Lungs of Mice by Intratracheal Instillation and Inhalation. *Environ. Toxicol.* **2007**, *22*, 415–421. [CrossRef] [PubMed]
118. Porter, D.W.; Hubbs, A.F.; Mercer, R.R.; Wu, N.; Wolfarth, M.G.; Sriram, K.; Leonard, S.; Battelli, L.; Schwegler-Berry, D.; Friend, S.; et al. Mouse Pulmonary Dose- and Time Course-Responses Induced by Exposure to Multi-Walled Carbon Nanotubes. *Toxicology* **2010**, *269*, 136–147. [CrossRef]
119. Totsuka, Y.; Higuchi, T.; Imai, T.; Nishikawa, A.; Nohmi, T.; Kato, T.; Masuda, S.; Kinae, N.; Hiyoshi, K.; Ogo, S.; et al. Genotoxicity of Nano/Microparticles in in Vitro Micronuclei, in Vivo Comet and Mutation Assay Systems. *Part. Fibre Toxicol.* **2009**, *6*, 23. [CrossRef]
120. Kim, J.K.; Shin, J.H.; Lee, J.S.; Hwang, J.H.; Lee, J.H.; Baek, J.E.; Kim, T.G.; Kim, B.W.; Kim, J.S.; Lee, G.H.; et al. 28-Day Inhalation Toxicity of Graphene Nanoplatelets in Sprague-Dawley Rats. *Nanotoxicology* **2016**, *10*, 891–901. [CrossRef]
121. Mendonça, M.C.P.; Soares, E.S.; de Jesus, M.B.; Ceragioli, H.J.; Irazusta, S.P.; Batista, Â.G.; Vinolo, M.A.R.; Maróstica Júnior, M.R.; da Cruz-Höfling, M.A. Reduced Graphene Oxide: Nanotoxicological Profile in Rats. *J. Nanobiotechnol.* **2016**, *14*, 53. [CrossRef]
122. Jain, S. Toxicity Issues Related to Biomedical Applications of Carbon Nanotubes. *J. Nanomed. Nanotechnol.* **2012**, *3*, 2. [CrossRef]

-
123. Raja, I.S.; Song, S.-J.; Kang, M.S.; Lee, Y.B.; Kim, B.; Hong, S.W.; Jeong, S.J.; Lee, J.-C.; Han, D.-W. Toxicity of Zero- and One-Dimensional Carbon Nanomaterials. *Nanomaterials* **2019**, *9*, 1214. [[CrossRef](#)]
 124. Yuan, X.; Zhang, X.; Sun, L.; Wei, Y.; Wei, X. Cellular Toxicity and Immunological Effects of Carbon-Based Nanomaterials. *Part. Fibre Toxicol.* **2019**, *16*, 18. [[CrossRef](#)] [[PubMed](#)]